2022

Hydrogeomorphic Response of Steep Streams following Severe Wildfire in the Western Cascades, Oregon

David Matthew Busby
University of Montana

HYDROGEOMORPHIC RESPONSE OF STEEP STREAMS FOLLOWING SEVERE WILDFIRE IN THE WESTERN CASCADES, OREGON

By

DAVID MATTHEW BUSBY

Bachelor of Science, State University of New York College at Oneonta, Oneonta, NY, 2017

Thesis

presented in partial fulfillment of the requirements
for the degree of

Master of Science
in Geosciences

The University of Montana
Missoula, MT

September 2022

Approved by:

Scott Whittenburg, Dean of the Graduate School
Graduate School

Dr. Andrew Wilcox, Chair
Department of Geosciences

Dr. Marco Maneta
Department of Geosciences

Dr. Philip Higuera
Department of Ecosystem and Conservation Sciences

Acknowledgements

I would like to thank my advisor, Andrew Wilcox, for providing me with guidance, encouragement, and independence, without which this thesis would not be possible. Thank you to my committee members, Marco Maneta and Phil Higuera, for their valuable perspectives and feedback. Thank you to my colleagues in the Geomorphology Lab Group, Claire Gilder and Jordan Gilbert, for their feedback on my research proposal and defense presentation, and to other students in the Geosciences Department for their support. Thank you to Nicole Cleland and Wendell Elliott for their assistance with field work. I am grateful to my research collaborators in Oregon. Kevan Moffett, Mark Sommer, and Cheryl Friesen were essential in gaining access and permissions to conduct field work. Josh Roering lent trail cameras and shared precipitation data. Mike Grilliot conducted a drone survey in the study area. Ben Vierra, Chris Burton, and Nick Harrison provided support for NEON data collection. Rich Grost, Becky McRae, and Ed Kikimoto provided reports on ground conditions in Oregon. Thank you to Vince Archer and Andy Efta for their guidance on project development. Jaylene Naylor assisted with drone survey logistics. Indy Singh provided administrative support. The Umpqua National Forest, the Willamette National Forest, the HJ Andrews Experimental Forest, and NEON provided access to study sites. This research was funded by the National Science Foundation, the North Umpqua Foundation, the Geological Society of America, and the UM Geosciences Department. Any opinions, findings, or conclusions expressed in this thesis are mine, and do not necessarily reflect those of funding sources.

Busby, David, M.S., Summer 2022 Geosciences

Hydrogeomorphic response of steep streams following severe wildfire in the Western Cascades, Oregon

Chairperson: Dr. Andrew Wilcox

Severe wildfire may alter the morphologic resilience of steep mountain streams by increasing peak discharges, elevating inputs of sediment and wood into channels, and increasing susceptibility to landslides and debris flows. In the Pacific Northwest, where mean annual precipitation is high and mean fire return intervals range from decades to centuries, understanding of steep stream response to fire is limited. In 2020, the Western Cascade Range, Oregon, experienced wildfire of historic magnitude and severity. The objective of this study was to evaluate the hydrologic and geomorphic response of steep streams to the 2020 fires. I assessed streamflow, instream wood, and changes in channel topography and bed-material size in steep stream reaches that burned in the fires and in an unburned reference reach. In the 1.5 years after the fires, peak flows in burned sites were below the two-year recurrence interval flood. A ~5-year flood in the unburned reference reach highlights the influence of other processes besides wildfire in driving streamflow in mountain watersheds. Sediment inputs to streams consisted of two large landslides initiated from road fill failure, slumps, sheetwash, and minor bank erosion. There was a 50% increase in the number of large wood pieces in burned sites after the fires. Changes in fluxes of water, sediment, and wood in burned streams induced shifts in the balance of sediment supply to transport capacity, initiating a sequence of sediment aggradation and bed-material fining followed by erosion and bed-material coarsening. Gross channel form showed resilience to change. The unburned reference reach exhibited little morphologic changes. Post-fire recruitment of large wood will have long-term implications for channel morphology and habitat heterogeneity. Anthropogenic climate change likely contributed to below-average precipitation during the study period which, combined with an absence of extreme precipitation events, was an important control on channel responses. Climate change may have a complex effect on stream response to wildfire by reducing total precipitation while simultaneously increasing susceptibility to flooding and debris flows via prolonged vegetation recovery and projected increases in extreme precipitation.

1. Introduction

Severe fire alters soil, vegetation, and hydrologic properties of mountain watersheds, commonly increasing inputs of water, sediment, and wood to stream channels for at least a year post-fire. This has implications for the form and function of steep mountain streams, which regulate flow and sediment to downstream water bodies and provide heterogeneous habitat. Hydrogeomorphic response of mountain streams to wildfire has been well studied in semiarid regions of the western United States, which have mean fire return intervals of years to decades (e.g., Minshall et al., 1997; Hoffman and Gabet, 2007; Florsheim et al., 2017; Chin et al., 2019). In the temperate Pacific Northwest, however, where fire return intervals range from decades to centuries, understanding of post-fire stream response is limited.

In 2020, the Western Cascade Range, Oregon, experienced historic wildfire. More area burned in the Oregon Cascades than in the previous 36 years combined, likely exceeding annual burned area since at least 1900 (Abatzoglou et al., 2021). The Archie Creek Fire and Holiday Farm Fire, which are the study areas for this research, burned over 1200 km^2 (Fig. 1), 74% of which burned at moderate or high soil burn severity (USGS and USFS, 2020). The Archie Creek Fire burned in an area characterized by a mixed and replacement severity fire regime with mean fire return intervals of 35–200 years. The Holiday Farm Fire burned in a stand replacement severity fire regime with return intervals of 200+ years (USGS, 2022a). The infrequency of severe wildfire in the Western Cascades is driven in part by a wet climate; the region receives 1.5–2.5 m of precipitation annually (PRISM, 2022). Both the Archie Creek and Holiday Farm fires were likely human-related ignitions (Carroll, 2021; Kavanaugh and Sickinger, 2020), enabled by extreme fuel aridity and driven by extreme winds during an east wind event (Abatzoglou et al., 2021).

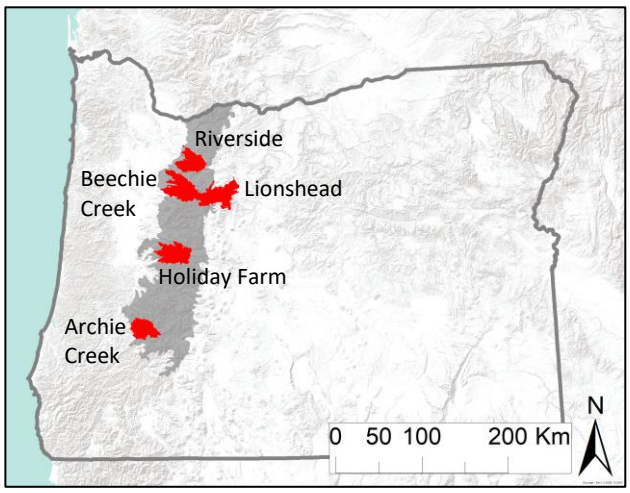

Figure 1. The five largest wildfires (red polygons) that burned in the Western Cascades, Oregon (shaded area) in 2020.

The historic magnitude and severity of the 2020 fires in the Western Cascades highlight the imperative to investigate the post-fire hydrogeomorphic response of mountain streams. High precipitation and prevalent steep topography suggest the region may be especially susceptible to post-fire flooding, landslides, and debris flows (McNabb and Swanson, 1990; Wondzell and King, 2003). While these events provide important sources of sediment and wood to steep streams over decadal time scales, in the short term these can threaten infrastructure, homes, and human lives (Jakob and Hungr, 2005) and disturb aquatic ecosystems, including spawning habitat for Endangered Species Act-listed Coho salmon (*Oncorhynchus kisutch*) and lamprey (*Petromyzontiformes*; FEMA, 2020). Historic timber harvest and associated road development in

areas burned in 2020 in western Oregon may also influence stream and watershed response to severe fire. Projected increases in fire activity across the Pacific Northwest under climate change (e.g., Littell et al., 2018; Halofsky et al., 2020) provide further impetus to evaluate the response of steep streams to the 2020 Oregon fires to enable informed post-fire hazard assessment and management in the future.

Steep mountain streams are shaped by infrequent landslide and debris flow deposits that restrict channel width and deposit large, immobile boulders in the channel (Grant et al., 1990). They are considered semi-alluvial in the sense that only a portion of the bed material can be reworked by fluvial bedload transport (Comiti and Mao, 2012). Boulders act as keystones upon which progressively smaller grains are stabilized from high flows, commonly resulting in the formation of steps (Grant et al., 1990; Church, 2006; Comiti and Mao, 2012). Other stabilizing channel bed structures include grain clusters and grain nets (Church, 2006). Stable bed structures foster resilience to moderate changes in discharge and sediment inputs following disturbance (e.g., Montgomery and Buffington, 1998). Sediment transport rates are often well below the theoretical maximum for the bulk sediments in the bed, and bedload finer than the structure-forming clast tends to be rapidly passed downstream (Montgomery and Buffington, 1998; Church, 2006). Although steep streams are resilient to moderate changes in water and sediment fluxes, they can exhibit dramatic changes during large floods (50- to 100-year events) and debris flows that exceed the threshold for mobilizing the large bed-forming grains (e.g., Montgomery and Buffington, 1997; Church, 2006).

Severe fire may alter the morphologic resilience of steep streams by changing fluxes of water, sediment, and wood in channels (Fig. 2). Increased overland flow and runoff in the years after fire is frequently attributed to (i) reduced surface storage capacity for rain due to the destruction of vegetation and litter, and (ii) increased soil water repellency (i.e., hydrophobicity) that reduces infiltration, but the latter is dependent on the amount and type of litter consumed and on the temperature reached (Shakesby and Doerr, 2006; Moody et al., 2013). Peak discharges can increase by up to two orders of magnitude in the immediate years following severe fire (Shakesby and Doerr, 2006), and subsequent failure of large wood jams can cause further increases (Neary et al., 2003). Floods of these magnitudes may be sufficient to destabilize bed structures and scour steep channels to bedrock (e.g., Germanoski and Miller, 1995; Chin et al., 2019).

Erosion is amplified in the years after intense fire due to the removal of vegetation and litter that exposes soil to raindrop impact and increases susceptibility to erosive overland flow as sheetwash or in rills and gullies. Post-fire mass movement processes include dry ravel, saturation-induced shallow landslides, and debris flows. Depending on the timing and intensity of post-fire rainfall events, there can be a delay of several years in the occurrence of post-fire landslides until after root systems have decayed and before new ones are established (Shakesby and Doerr, 2006). Shallow landslides during heavy rainfall can initiate debris flows (Shakesby and Doerr, 2006), which is the dominant post-fire debris flow initiation mechanism in wet regions like the Pacific Northwest (e.g., Benda, 1990). Alternatively, debris flows can be runoff-initiated, whereby overland flow and rill erosion in steep headwaters leads to

progressive accumulation of sediment (i.e., progressive bulking) and deep incision in shallower channels (Meyer and Wells, 1997). These diverse erosion mechanisms can produce increases in sediment yield of up to four orders of magnitude following fire (Moody and Martin, 2009).

Increased erosion and sediment inputs following fire can cause transport-limited conditions in steep streams and subsequent aggradation (e.g., Keller et al., 1997; Florsheim et al., 2017). Fine sediment accumulation followed by scouring may mobilize large bed-forming grains. Transport of coarse gravels may also destabilize the bed by impacting large grains at rest (Recking et al., 2012). Landslides and debris flows scour sediment and organic material from hillslopes and headwater channels and can deposit significant amounts of mixed fine and coarse sediment and large wood at junctions with steep streams. This can inflict diverse changes to channel morphology upstream and downstream of the debris fan (e.g., Benda, 1990; Benda et al., 2003a; Hoffman and Gabet, 2007). Large wood can also be supplied to mountain streams from post-fire treefall and bank erosion (e.g., Minshall et al., 1997; Benda et al., 2003b). By increasing flow resistance and reducing sediment transport capacity (e.g., Montgomery et al., 2003), large wood jams can cause substantial aggradation of post-fire sediment inputs (Short et al., 2015; Wohl et al., 2022).

Fire-induced changes to water, sediment, and wood fluxes and associated channel response are highly variable across regions and watersheds due to interacting climatic, biophysiographic, and anthropogenic factors (e.g., Benda and Dunne, 1997; Shakesby and Doerr, 2006; Moody et al., 2013). Influential factors include burn severity and extent, precipitation (magnitude, duration, intensity), channel and basin morphology (e.g., gradient, confinement), vegetation (type, coverage, rate of regrowth), soils (type, thickness), lithology, and land management (e.g., timber harvest, road construction) (e.g., Swanson, 1981; Sidle et al., 1985; McNabb and Swanson, 1990; Montgomery and Buffington, 1998; Cerda and Doerr, 2005; Shakesby and Doerr, 2006; Moody et al., 2013; Vieira et al., 2015; Fig. 2). The myriad of factors that influence stream response to wildfire (Fig. 2) drives the need for cross-catchment investigations that may elucidate the fundamental drivers of morphologic change in steep streams.

The objective of this study was to evaluate the hydrologic and geomorphic response of steep streams to severe wildfire in the Western Cascades. To do so, I assessed streamflow, instream wood, and post-fire changes in channel topography and bed-material size in four steep stream reaches that burned in the 2020 wildfires, and I compared observations to conditions in an unburned reference reach and nearby gaged streams. I assessed post-fire precipitation, sediment inputs, and flow competence to contextualize hydrogeomorphic responses. Further, I explored observed channel responses in the context of variable site characteristics to provide insight on the potential controls on post-fire responses. This work advances understanding of watershed response to extreme fire in a region that is increasingly susceptible to disturbance and has implications for post-fire hazard mitigation and management.

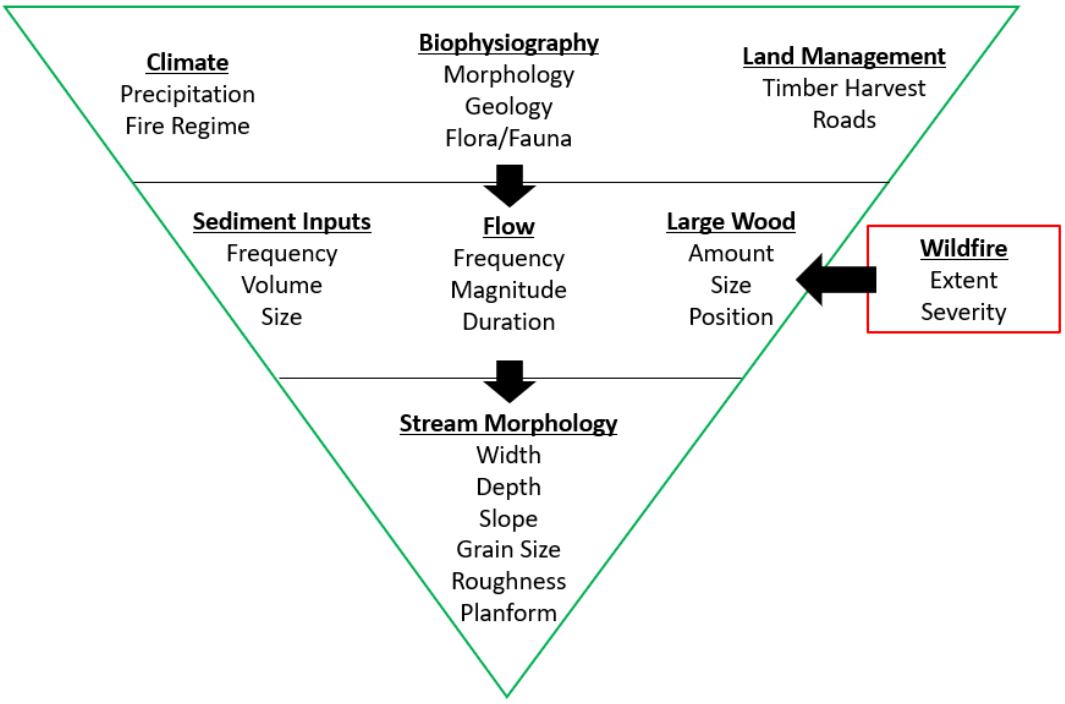

Figure 2. Conceptual figure illustrating the role of wildfire as a disturbance in mountain watersheds. Green triangle illustrates the tiered controls on steep stream morphology in a mountain watershed characteristic of the study area that existed prior to the 2020 wildfires. Wildfire (red rectangle) alters sediment, flow, and large wood regimes, thereby influencing stream morphology.

2. Study Area

I have four burned study sites within the Archie Creek and Holiday Farm fires in the Western Cascades (Fig. 3). The Western Cascade Range flanks the western slope of the Oregon Cascades and is distinct from the High Cascades Range which runs along the crest. The Western Cascades comprise a Miocene-upper Eocene volcanic arc, with dacitic tuffs, andesite lava flows, and lesser basaltic and rhyolitic volcanic rocks (Conrey et al., 2002). Dissection is driven by glacial erosion, streams fed by shallow subsurface stormflow, and debris flows, producing a landscape with steep slopes and extensive drainages (Jefferson et al., 2010). Relatively high rates of runoff and erosion (FEMA, 2020) provide substantial bed material to rivers (O'Connor et al., 2014). Both the Archie Creek and Holiday Farm fires straddled the boundary of the foothills and the steeper, high relief interior of the Cascades and engulfed large east-west lying rivers, the North Umpqua River and McKenzie River, respectively. The North Umpqua and McKenzie rivers are important regional rivers for water supply and salmon fisheries. Steep tributary streams flow north and south linking steep ridges with the gentler McKenzie River and North Umpqua River valleys.

I selected study sites that I hypothesized to have high propensity for geomorphic change from post-fire runoff and erosion. As such, study basins have predominantly steep gradients and moderate and high soil burn severity (Fig. 3; Table 1), meaning that nearly all the organic

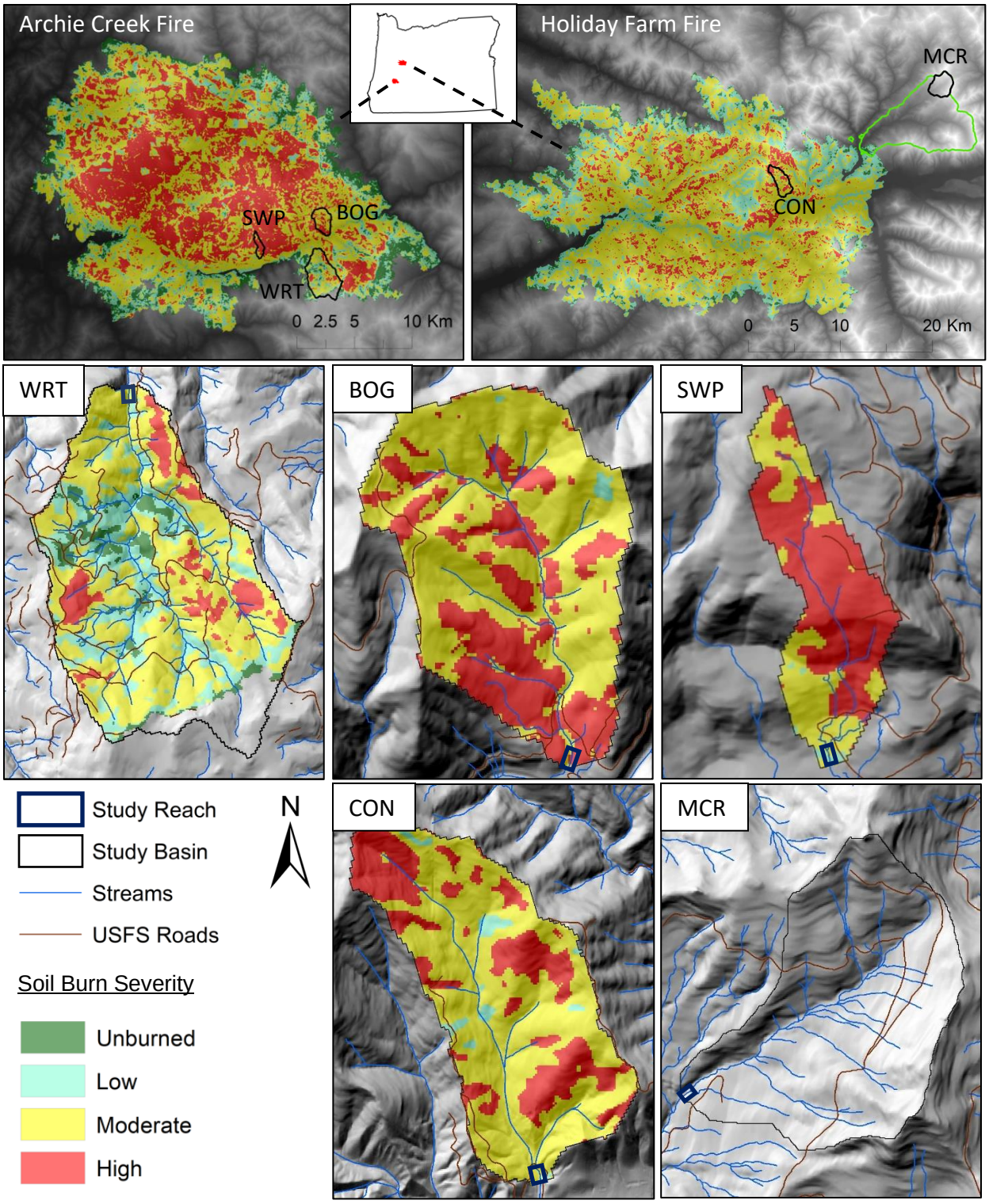

Figure 3. Soil burn severity maps of the study area. Top row: burn severity of the Archie Creek Fire and Holiday Farm Fire with labeled study basin locations. Green polygon denotes HJ Andrews Experimental Forest. Inset map indicates the location of the fires in Oregon. Middle and bottom rows: burn severity of study basins showing streams, roads, and study reach location.

ground cover was consumed by the fire. Within basins I selected a single steep stream reach with a ~5–10% gradient for repeat surveys of channel morphology. Reaches are in 3rd and 4th order streams (Table 1) in the vicinity of junctions with headwater tributaries, corresponding to locations in the stream network more frequently subject to landslide and debris flow deposits (e.g., Benda et al., 2003a; Bigelow et al., 2007). Study reaches are also within or near channel segments predicted to have high debris flow hazard in response to a 15-min, 24 mm hr^{-1} rainfall intensity by the United States Geological Survey (USGS, 2020). Wright Creek, Bogus Creek, and Swamp Creek burned in the Archie Creek Fire and are tributaries of the North Umpqua River. Cone Creek burned in the Holiday Farm Fire and is a tributary of the McKenzie River. When initiating this study in late 2020, following the fires, selection of burned study sites was severely constrained by accessibility and safety concerns. I also have one unburned reference site, McRae Creek, to enable a comparison of post-fire responses between burned and unburned sites. McRae Creek is located 8 km northwest of the Holiday Farm Fire in the HJ Andrews Experimental Forest (Fig. 3) and is a National Ecological Observation Network (NEON) site with continuous records of stage and discharge and pre-fire channel morphology data. I use the following codes for my study sites: WRT (Wright Creek), BOG (Bogus Creek), SWP (Swamp Creek), CON (Cone Creek), and MCR (McRae Creek).

Study basins have variable timber harvest histories (Table 1), the primary method of which was stand clearcutting. Only BOG has been harvested after 1998; this was a small salvage logging operation following the 2009 Williams Creek Fire which burned nearly all of the catchment at mixed severity (USFS, 2022; USGS and USFS, 2022). 30% of WRT burned at low severity in the 2017 Nu Fall Creek Fire (USGS and USFS, 2020), but this did not impact forested area, which was 100% prior to the Archie Creek Fire (USGS, 2022a; Table 1). Study basins exhibit similar variability in density of logging roads, with WRT having the greatest road density of 2.4 km km^{-2} (USFS, 2022; Table 1; Fig. 3). Prior to the fire, forested areas were dominated by Douglas-fir (*Pseudotsuga menziesii*) and western hemlock (*Tsuga heterophylla*; USGS, 2022a). Mean annual precipitation in study basins is high, ranging from ~1.5 to 2.2 m (PRISM, 2022; Table 1). Most precipitation occurs during the winter as rain during long-duration, low-intensity frontal storms, with mixed rain and snow above ~600 m in elevation. The largest floods are generated by late-winter rain-on-snow events (FEMA, 2020). Summers are relatively warm and dry. Characteristic organic matter-rich loam soils have a high infiltration capacity, making infiltration-excess overland flow rare even after severe fire. Dry ravel and saturation-induced shallow landslides and debris flows are the dominant post-fire mass wasting processes in the region (Wondzell and King, 2003; Jackson and Roering, 2009). However, a single runoff-initiated debris flow was documented in the Western Cascades following the 2017 Milli fire (Wall et al., 2020).

Study reaches are predominantly cobble- and boulder-bedded and exhibit stepped-bed morphologies, characteristic of stable steep streams. WRT and CON are bisected by steep gullies rated with high and moderate debris flow hazard, respectively. SWP is bisected by a perennial tributary with high debris flow hazard (USGS, 2020).

Table 1. Characteristics of study sites.

	WRT	BOG	SWP	CON	MCR
Fire	Archie	Archie	Archie	Holiday	N/A
Reach Slope[a] (%)	4.8	6.0	10.0	5.9	6.2
Reach Length[a] (m)	71	116	116	107	53
Reach Elevation[b] (m)	328	306	410	352	884
Reach Burn Severity[c]	mod	mod/high	mod	mod	N/A
Stream Order	4	4	3	4	3
Drainage Area[b] (km^2)	8.9	2.8	1.1	4.5	4.2
Mean Basin Slope[b] (%)	45	56	30	51	39
Mean Basin Elevation[b] (m)	884	646	762	747	1250
Basin Relief[b] (m)	1010	628	622	945	713
Harvested Area[d] (%)	48	1	27	0	21
Pre-fire Forested Area[e] (%)	100	59	79	100	100
Road Density (km km^{-2})[f]	2.4	1.0	1.2	0.7	1.6
Mean Annual Precip.[g] (m)	1.6	1.5	2.0	2.1	2.2
% High Burn Severity[h]	9	34	64	30	N/A
% Moderate Burn Severity[h]	52	65	35	68	N/A
% Low Burn Severity[h]	24	1	1	3	N/A
% Unburned[h]	14	0	0	0	N/A

[a] From initial topographic surveys.
[b] Source: USGS (2022b).
[c] Soil burn severity adjacent to study reach (USGS and USFS, 2020).
[d] Percent of catchment area that has been harvested in the past. May not include all historic harvest activity (USFS, 2022).
[e] Source: USGS (2022a).
[f] Source: USFS (2022).
[g] Source: PRISM (2022).
[h] Soil burn severity of study basin as percent of total area (USGS and USFS, 2020).

3. Methods

3.1. Field Surveys

To measure post-fire hydrogeomorphic responses, I conducted repeat field surveys in the 1.5 years after the wildfires. I was first able to access the burned areas in mid-December 2020 (Dec-20), 1.5 months after the fires were contained, but 3 months after most of the fire spread. This was following a 24-hour, 76 mm and 58 mm rain event in mid-November near my Holiday Farm Fire and Archie Creek Fire study sites, respectively, as recorded by rain gages installed by research collaborators. Field observations in Dec-20 suggest that this rain event altered stream morphology from pre-fire conditions. I conducted repeat surveys in June 2021 (Jun-21) and March 2022 (Mar-22). I surveyed my unburned reference reach, MCR, in Jun-21 only. This study

period encompassed two winters, when most precipitation occurs in the study area and there is the greatest chance of landslides and debris flows.

During each field visit, I used a Leica TS06 total station and an Emlid Reach GPS receiver to conduct georeferenced surveys of 5–11 cross-sections per reach and longitudinal profiles of the thalweg (Figs. A1–A5). To characterize grain size of the mobile clasts, I completed Wolman pebble counts of ~100 grains, excluding boulders (Wolman, 1954). An additional pebble count was conducted in WRT to characterize the influence of large wood jams on modulating bed grain size. I measured discharge during each field visit using a SonTek FlowTracker ADV. I installed an In-Situ Level TROLL 300 pressure transducer in each ungaged site to record stage at 15-minute intervals, and barometric pressure transducers adjacent to WRT and CON to correct for atmospheric pressure. To document daily stream conditions and high flow events, Browning Recon Force trail cameras were mounted to tree trunks and directed at streams, large wood jams, and gullies. Cameras were motion-triggered and took two photos per day. MCR has a permanent trail camera that takes a photo every 30 minutes during daylight. Finally, I took photos along the length of study reaches to document changes in stream morphology, large wood, and point sources of sediment.

I used uncrewed aerial vehicle (UAV, i.e., drone) surveys to further characterize stream and hillslope conditions and to document any large mass wasting events that provided sediment to study streams. An initial UAV survey of BOG was completed by the University of Washington Natural Hazards Reconnaissance (RAPID) Facility in March 2021. I conducted additional UAV surveys of burned sites in Jun-21 and Mar-22 using a DJI Mavic 2 Pro. I georeferenced drone surveys by surveying ground control points with GPS.

3.2. Precipitation

To quantify precipitation, one of the potential controls on channel response to fire (Fig. 2), I used a combination of data from tipping-bucket rain gages installed by research collaborators, USGS meteorological stations, and the PRISM Climate Group (Table A3). For water years (WYs) 2021 and 2022, I estimated total precipitation, percent of normal precipitation, and Z-scores of total precipitation, or the number of standard deviations away from the mean. I also calculated maximum daily precipitation and maximum 24-hour precipitation, the latter of which has been used to characterize debris flow thresholds in western Oregon (Wiley, 2000). Finally, I calculated the maximum 15-minute rainfall intensity, a metric used by the USGS to characterize debris flow hazard (USGS, 2020).

3.3. Hydrologic Response

To evaluate the hydrologic response of steep streams to the 2020 wildfires, I assessed peak flow stage and discharge in study reaches. I used pressure transducer and cross-section measurements to determine the duration of flows exceeding bankfull, which has been shown to be a geomorphically effective flow in alluvial channels (Wolman and Miller, 1960). In ungaged streams, I estimated peak discharges during the portion of WYs 2021 and 2022

encompassed by my study period by first back-calculating Manning's *n* roughness coefficient using field discharge and topographic measurements and the discharge form of the Manning equation:

$$n = \frac{R^{2/3} S^{1/2} A}{Q} \quad (1)$$

where *R* is hydraulic radius, *S* is slope, *A* is wetted area, and *Q* is discharge. Using my estimates of Manning's *n* and *R* and *A* values calculated at the pressure transducer during the peak stage, I rearranged equation 1 to solve for the peak discharge.

I also estimated peak discharges using one-dimensional hydraulic modeling in HEC-RAS (Hydrologic Engineering Center's River Analysis System). HEC-RAS requires cross-section geometries, Manning's *n*, and discharge, and outputs a water surface elevation profile and hydraulic metrics (e.g., flow depth, shear stress) at each cross-section for the modelled flow. I used cross-section geometries from Mar-22 field surveys. I calibrated Manning's *n* by simulating field discharges from Dec-20 and Mar-22. Then, I assumed that Manning's *n* stayed constant at greater flows, and varied discharge until the modeled water surface matched the water surface recorded by the pressure transducer during the peak flows in 2021 and 2022 (additional details on HEC-RAS model calibration, simulations, and error assessment are provided in the appendix). I compared timing, magnitude, and recurrence intervals (estimated using USGS regression relations; USGS, 2022b) of peak discharges in study streams to those in both burned and unburned gaged creeks in HJ Andrews Experimental Forest and nearby USGS gaged streams.

3.4. Geomorphic Response

To evaluate the geomorphic response of steep streams to the 2020 wildfires, I quantitatively assessed changes in channel topography and bed-material size in burned sites for three time periods: Dec-20 to Jun-21, Jun-21 to Mar-22, and Dec-20 to Mar-22. I calculated the percent change in reach-averaged bankfull width and depth during each time period and tested for significant differences using the non-parametric Wilcoxon rank sum test, which is applicable to small sample sizes and non-normally distributed data. I evaluated changes in channel longitudinal geometry by calculating the change in reach slope and bed roughness height, as characterized by the standard deviation of the thalweg elevation (Coleman et al., 2011). To assess changes in channel bed material, I calculated the percent change in the D_{50}, the grain size below which 50% of the bed material is finer. I tested for significant differences in grain size distributions during each time period using the Kolmogorov-Smirnov test. All statistical analyses were performed in R. In MCR, which I surveyed in Jun-21 only, I repeated cross-section and pebble count measurements taken by NEON staff in August 2019 and evaluated change between 2019 and 2021 (additional details on MCR sampling and analyses are provided in the appendix). The period from August 2019 to June 2021 is similar to my study period in that it encompasses two winters in which flows at nearby gages were predominantly below the two-year recurrence interval flood. As such, I considered the change in MCR between 2019 and

2021 as representative of the magnitude of change that may have occurred during my study period.

To contextualize temporal changes in bed grain size and channel geometry in study sites, I assessed sediment inputs to streams and flow competence. I used three-dimensional point clouds developed from UAV imagery with Pix4D Mapper software to estimate volumes of sediment supplied to study streams from post-fire mass wasting events. I assessed flow competence (i.e., the ability of flow to mobilize bed material) by comparing boundary shear stress during the peak flow in WYs 2021 and 2022 to the critical shear stress needed to transport the D_{50}. In burned sites, I assessed flow competence at each surveyed cross-section using boundary shear stress values from HEC-RAS modeling. In MCR, for which I did not run HEC-RAS, I calculated boundary shear stress, τ_0, at the pressure transducer cross-section during the peak flow using the equation:

$$\tau_0 = \rho g R S \tag{2}$$

where ρ is water density and g is acceleration due to gravity. I calculated the critical shear stress, τ_c, for mobilization of the D_{50} as:

$$\tau_c = \tau_c^*(\rho_s - \rho)gD \tag{3}$$

where τ_c^* is the dimensionless critical shear stress and ρ_s is sediment density. To estimate τ_c^*, I used a slope-dependent equation that accounts for changing hydraulics in steep streams (Recking, 2009), and which was independently obtained in three studies using different methods (Recking et al., 2012):

$$\tau_c^* = 0.15S^{0.275} \tag{4}$$

Finally, I calculated τ_0/τ_c. For entrainment of the D_{50} to occur, τ_0 must be greater than τ_c, i.e., the ratio must be greater than one. I also estimated the maximum grain size that was mobilized during the peak flow using equation 3 by plugging τ_0 in for τ_c and solving for D.

3.5. Instream Wood

To provide insight on the influence of wildfire on instream large wood and associated effects on channel morphology, I assessed large wood conditions in burned sites in Mar-22 and in MCR in Jun-21. To do so, I used a combination of ground photos and analysis of high-resolution (<4 cm pixel resolution), georeferenced orthophotos developed from UAV imagery in Pix4D Mapper. I considered large wood to be any piece with a mid-length diameter ≥20 cm (the size that could be readily identified in orthophotos) that extended at least 1 m into the bankfull channel. I classified each piece as single or part of a jam (defined as three or more pieces of large wood in contact), and noted the presence or absence of a rootwad, features of accumulation, level of decay, burn status, stability, source, and whether the piece forced a geomorphic unit (e.g., pool, bar) and was storing sediment (Wohl et al., 2010). I also used repeat photos and trail

camera time-lapse photos to qualitatively assess changes in large wood in burned sites over the study period.

4. Results

To provide visual accompaniment for the following results, videos from UAV surveys in burned study sites can be accessed here: https://www.youtube.com/playlist?list=PLol1sSNkuqpQJzG9za0gusQCsDzRdJeIs.

4.1. Precipitation

Most precipitation during the study period occurred between the months of October and April (Fig. 4). Trail camera time-lapse photos indicate that precipitation fell mostly as rain in study sites, with slightly more snow in the higher elevation MCR site. Total precipitation during WY 2021 and the portion of WY 2022 encompassed by my study period was below average in all sites, although Z-scores of log-transformed total precipitation were greater in WY 2022 and sites near the Holiday Farm Fire (CON and MCR) had greater Z-scores than Archie Creek Fire sites. In WYs 2021 and 2022, Z-scores in Archie Creek Fire sites ranged from -1.7 to -1.4 and -0.90 to -0.74, respectively. Z-scores in sites near the Holiday Farm Fire ranged from -0.87 to -0.83 and -0.60 to -0.57 in WYs 2021 and 2022, respectively (Table 2). Timing of the maximum daily rain event showed some variability, although in WY 2022 it occurred on either 4 or 5 January 2022 at all sites. In Archie Creek Fire sites, maximum daily precipitation was greater in 2022 than in 2021. The opposite pattern is true for sites near the Holiday Farm Fire. There was similar variability in timing of the maximum 15-minute rainfall intensity, which ranged from 17 to 21 mm hr^{-1} during the study period (Table 2). Due to variability in data sources and proximity of gages to study sites (Tables 2 and A3), rainfall data presented here are approximations of actual values.

Table 2. Precipitation (ppt) and precipitation intensity (PI) data in WYs 2021 and 2022.

		WRT	BOG	SWP	CON	MCR
Total ppt[a] (mm)	WY 2021	1191	1134	1414	1786	1851
	WY 2022[b]	811	752	987	1290	1333
% of normal ppt[a, c]	WY 2021	74	75	71	84	83
	WY 2022[b]	81	79	78	84	84
Z-score of log(total ppt)[a, c, d]	WY 2021	-1.5	-1.4	-1.7	-0.83	-0.87
	WY 2022[b]	-0.74	-0.84	-0.90	-0.60	-0.57
2021 max daily ppt	ppt (mm)	37[e]	37[e]	37[e]	65[f]	65[f]
	Date	11/18/20	11/18/20	11/18/20	12/20/20	12/20/20
2022 max daily ppt[b]	ppt (mm)	49[a]	47[a]	59[a]	59[g]	59[g]
	Date	1/4/22	1/4/22	1/4/22	1/5/22	1/5/22
2021 max 24-hour ppt	ppt (mm)	58[e]	58[e]	58[e]	80[f]	80[f]
	Date	11/15/20	11/15/20	11/15/20	12/20/20	12/20/20
2022 max 24-hour ppt[b, h]	ppt (mm)	–	–	–	67[g]	67[g]
	Date	–	–	–	1/5/22	1/5/22
2021 max 15-min PI	PI (mm hr^{-1})	17[e]	17[e]	17[e]	21[g]	21[g]
	Date	1/13/21	1/13/21	1/13/21	9/18/21	9/18/21
2022 max 15-min PI[b, h]	PI (mm hr^{-1})	–	–	–	17[g]	17[g]
	Date	–	–	–	11/10/21	11/10/21

[a] Source: PRISM (2022).
[b] For the portion of WY 2022 encompassed by my study period (Oct. 2021–Mar. 2022).
[c] Based on the period since 1982.
[d] Precipitation is a log-normally distributed metric, so I report Z-scores of the log-transformed total precipitation.
[e] Source: Archie1 tipping bucket gage.
[f] Source: Holiday4 tipping bucket gage.
[g] Source: USGS Blue River Dam Met Station near Blue River, OR, #441016122194300.
[h] No data available for Archie Creek Fire sites at a resolution finer than daily.

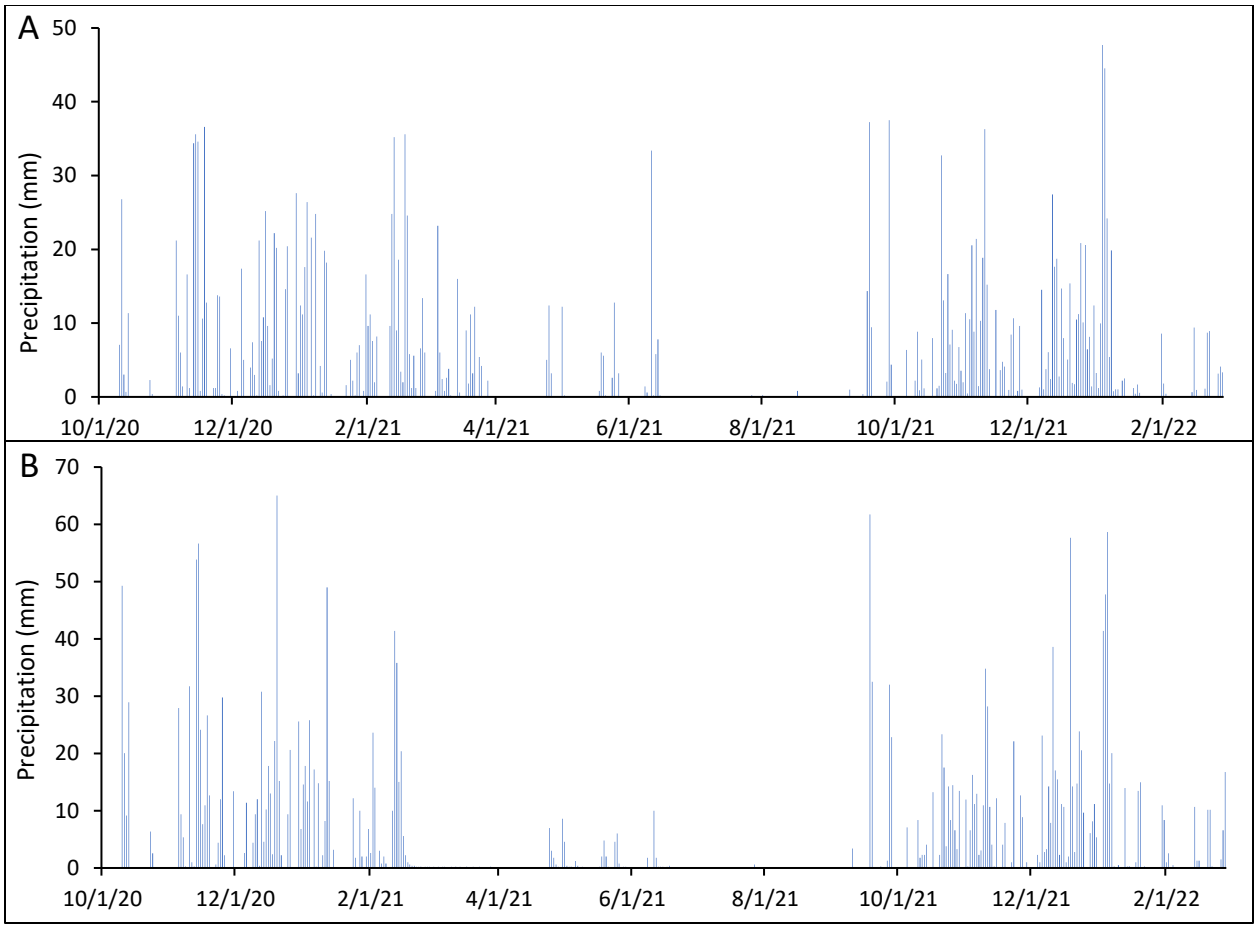

Figure 4. Daily precipitation for WY 2021 and the portion of WY 2022 encompassed by my study period near (A) Archie Creek Fire and (B) Holiday Farm Fire study sites. Data are from a mix of tipping-bucket gages, USGS gages, and PRISM. Y-axis scales differ.

4.2. Hydrologic Response

The bulk of streamflow during the study period occurred between the months of October and April. Storms caused rapid increases in stage that produced flashy hydrographs in burned sites (Fig. 5). Flow in MCR was less flashy (Fig. 5), perhaps due to less overland flow during storm events and a greater amount of precipitation falling as snow. Identification of peak flows during WYs 2021 and 2022 showed that there were sometimes up to three distinct peaks in the stage hydrograph within 1 cm of the highest recorded stage (Fig. 5); I thus considered each of these in order to better characterize discharge and associated flow competence. There was variability in the timing of peak flows among Archie Creek Fire sites in WY 2021. Flows in CON and MCR peaked on 20 December 2020. In WY 2022 flows in all sites peaked from 5 to 7 January 2022 (Table 3; Fig. 5). Despite some variability, timing of peak flows in study streams was mostly consistent with those in unregulated gaged streams within 25 km of my sites (Tables 3, A7, and A8).

Peak discharge estimates from the back-calculation method sometimes varied substantially due to differences in Manning's *n* estimates at different cross-sections and flows (Tables 3 and A5). Discharge estimates from HEC-RAS modeling were within the range of back-calculations (Table 3) and were used for subsequent calculations of unit area discharge and flow competence. Because substantial flow in SWP was conveyed beneath undercut banks that could not be accurately surveyed (Figs. 9 and A16), I was unable to back-calculate peak discharges or build a representative HEC-RAS model in SWP. Peak flows in Archie Creek Fire sites were greater in 2022 than in 2021 (Table 3), which is mostly consistent with nearby gaged streams (Table A7). Peak flows in CON were also greater in 2022, while the opposite is true for nearby gaged streams, including MCR (Tables 3 and A8).

Except for MCR, peak unit discharges in study streams were consistently below those measured at nearby gages. Streamflow regression relations developed for Oregon by the USGS suggest that the 2021 peak flow in MCR had a ~5-year recurrence interval, while flows in other study sites and nearby gaged sites were mostly below the two-year flood (USGS, 2022b; Tables 3, A7, and A8). Except for CON and MCR, flows remained below bankfull level in 2021 and 2022 at the pressure transducer cross-sections (Fig. A7). In CON, stage exceeded bankfull level for one hour on 6 January 2022. In MCR, stage exceeded bankfull for a cumulative time of ~20 days in 2021 and ~11 days in 2022. HEC-RAS modeling indicates that flows exceeded bankfull conditions at select cross-sections in BOG and CON in 2021 and 2022 and in WRT in 2022. That flows largely remained confined to the bankfull channel is consistent with field observations and time-lapse photos.

Table 3. Peak discharge (Q) and recurrence interval (RI) data at study sites.

Site	Water Year	Date of Peak Q	Estimated Peak Q (m^3/s)		Final Q Estimate[a] (m^3/s)	Peak Unit Area Q*10^8 [(m^3/s)/m^2]	Flood RI[b] (yrs)
			Back-Calculation	HEC-RAS			
WRT	2021	1/13/21 2/13/21 2/19/21	0.7 – 1.1	0.9	0.9	10	<2
	2022	1/5/22	1.0 – 1.6	1.3	1.3	15	<2
BOG	2021	12/17/20 12/20/20 2/13/21	0.3 – 0.8	0.5	0.5	18	<2
	2022	1/6/22	0.5 – 1.4	0.6	0.6	21	<2
SWP	2021	2/18/21	–	–	–	–	–
	2022	1/7/22	–	–	–	–	–
CON	2021	12/20/20	0.9 – 1.9	1.1	1.1	24	<2
	2022	1/6/22	1.2 – 2.7	1.9	1.9	42	<2
MCR	2021	12/20/20	–	–	4.7	110	~5
	2022	1/6/22 3/3/22	–	–	1.5	36	<2

[a] Used HEC-RAS estimation of Q for burned sites. Values in MCR determined from stage-discharge relation.

[b] Source: USGS (2022b).

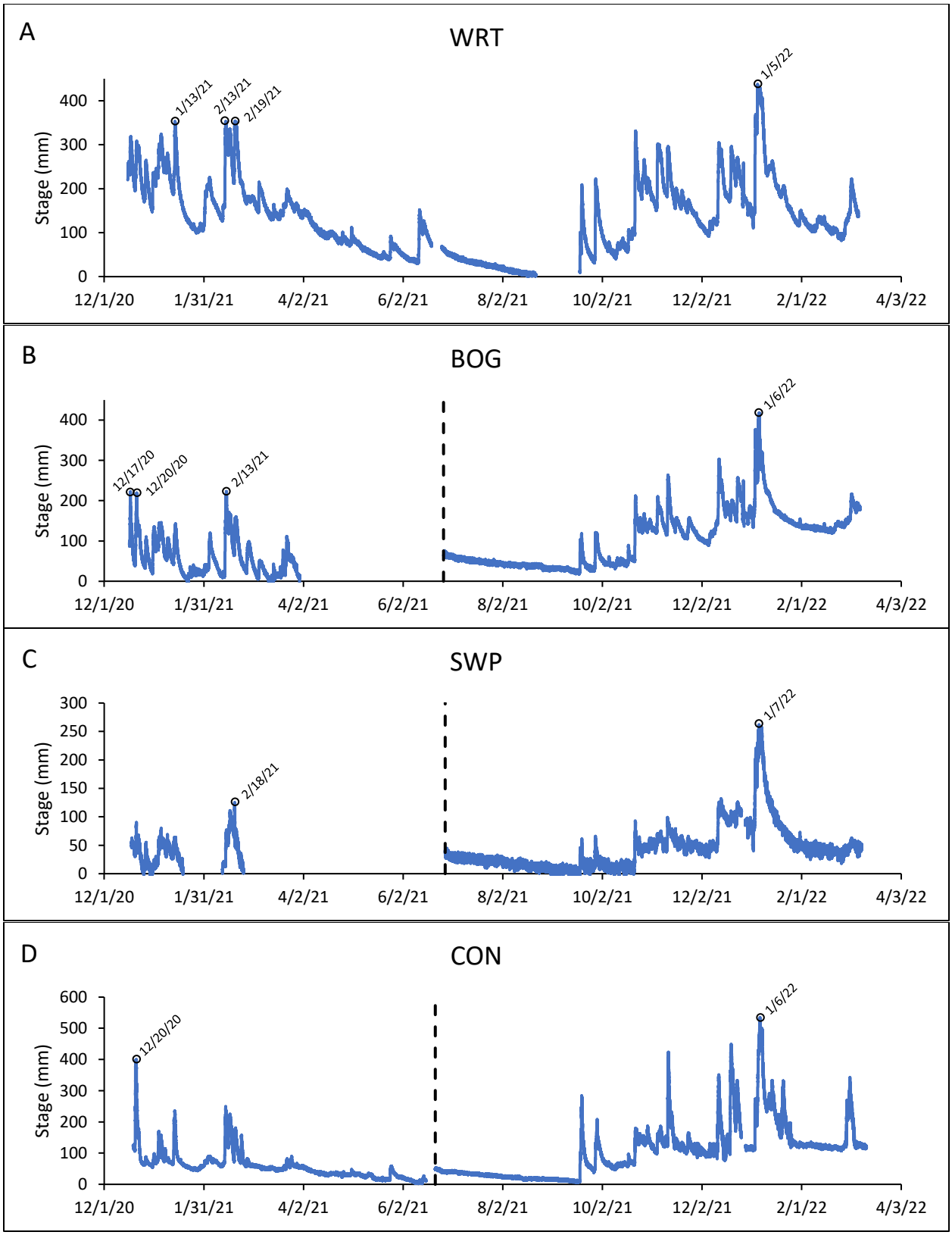
A
WRT
Stage (mm)
1/13/21
2/13/21
2/19/21
1/5/22
B
BOG
12/17/20
12/20/20
2/13/21
1/6/22
C
SWP
2/18/21
1/7/22
D
CON
12/20/20
1/6/22
12/1/20
1/31/21
4/2/21
6/2/21
8/2/21
10/2/21
12/2/21
2/1/22
4/3/22

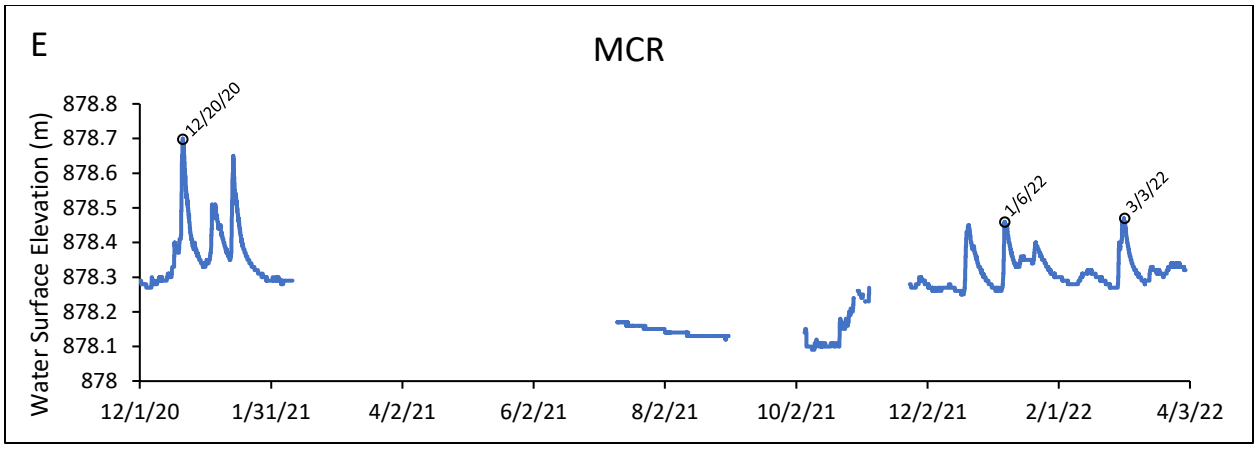

Figure 5. Time series of stage (measured from pressure transducer sensor; A-D) and water surface elevation (E) in study sites. Data gaps indicate measurement error or when the transducer was not submerged. For MCR, peak flow dates at nearby gages in the HJ Andrews Experimental Forest (Table A8) suggest that the available record captures peak flows for WYs 2021 and 2022. Black circles mark distinct flow peaks within 10 mm of the highest recorded stage for each WY. Vertical dashed line indicates a change in the transducer location. Y-axis scales differ.

4.3. Sediment Inputs to Study Streams

Post-fire erosion in study sites was mostly minor. Following the first winter rainy season after the fires, there was little sediment accumulation above culverts at road crossings upstream of study reaches, suggesting that the delivery of sediment to my reaches was not impeded. I documented two large mass-wasting events that supplied sediment to study streams. Both were landslides that occurred ~600 and 700 m upstream of WRT on 4 January 2022 (Fig. 6A). The slides were triggered by fill failure on Wright Creek Road (Figs. 6 and A8) during a 1-day, 49 mm rain event (Table 2). The landslide further upstream occurred in a tributary gully rated with high debris flow hazard (USGS, 2020) and eroded ~900 m^3 of sediment, in some places scouring to bedrock. The sediment delivery ratio (SDR) was 83%, with ~750 m^3 of sediment entering the stream (Table A9). The debris fan was comprised mostly of fine sediment and large wood (Figs. 6C and A9). The fan forced a channel constriction, forming a large pool on the upstream side below which was a steep drop (Fig. A9). The downstream landslide had a volume of ~1200 m^3 and deposited a debris fan of mostly cobble and boulder-sized sediment and some large wood adjacent to the creek (Table A9; Fig. 6E). The SDR was 25%, with ~300 m^3 of sediment entering the stream (Table A9).

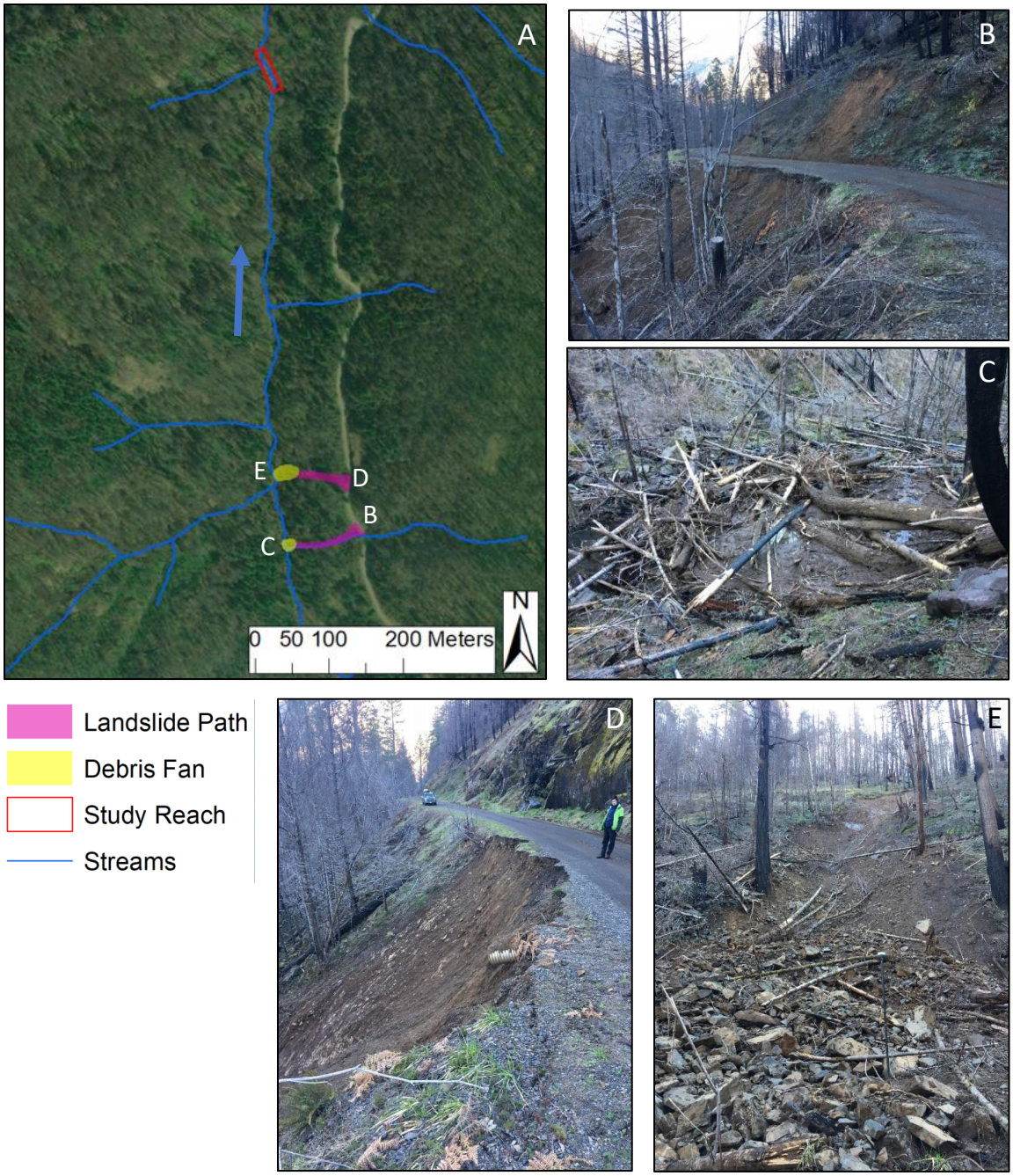

Figure 6. Landslides in Wright Creek basin triggered from road fill failure on 4 January 2022. (A) Post-fire aerial photo indicating landslide, stream, and study reach locations. Blue arrow indicates flow direction. Text denotes locations of ground photos: (B) upstream landslide initiation zone; (C) upstream landslide debris fan of mostly fine sediment and large wood; (D) downstream landslide initiation zone; and (E) downstream landslide debris fan of cobble to boulder-sized sediment and large wood.

Trail camera time-lapse photos showed increased turbidity during high flows in burned sites (Figs. 7, A11, and A12), likely from fine sediment inputs from burned hillslopes. Comparing

timing of turbid flows to precipitation data suggests erosive overland flow occurred during storms exceeding a 24-hour, ~1.6 mm hr^{-1} intensity. I also noted overbank fine sediment deposition in BOG and CON in the initial 1.5 months after the fires (Fig. A13). Increased turbidity was not observed in MCR during the peak flows. UAV surveys and field observations revealed little evidence of rilling and gullying on burned slopes, suggesting that erosive overland flow occurred mainly as sheetwash. However, I identified one rill just upstream of BOG during initial surveys that deposited a small fan of fine to cobble-sized sediment on the floodplain (Fig. A14), although it is unknown if the rill developed post-fire. I documented three slumps along channel margins that supplied sediment to study sites. The first occurred in BOG during the initial 1.5 months after the fires (Fig. 8). Two other slumps occurred at the downstream end of CON during the second winter rainy season after the fires (Fig. A10). Bank erosion did not appear to be a large source of sediment to study reaches. There were isolated cutbanks in BOG (Fig. A15), CON, and MCR, but little evidence of erosion during the study period. There were recently fallen trees along the channel margin in BOG (Fig. 8) and WRT. SWP was the most visibly unstable of my study streams. In some places the stream was deeply incised with steep and undercut banks of exposed soil (Fig. 9). I documented recent bank

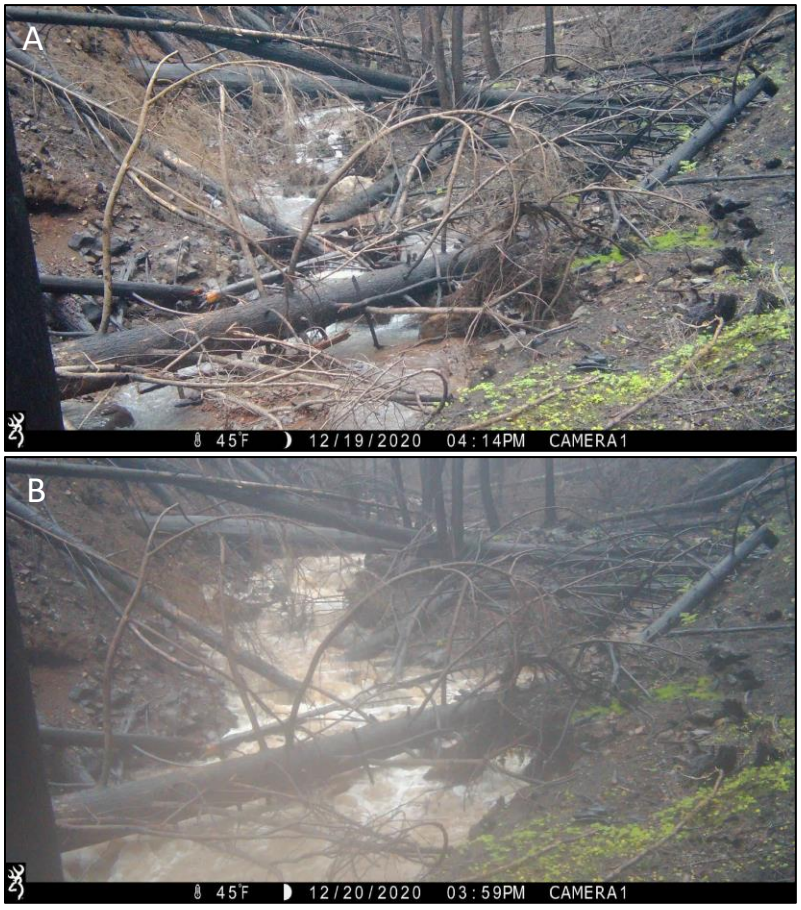

Figure 7. Trail camera time-lapse photos looking just upstream of BOG showing flow (A) the day before and (B) the day of the peak flow on 20 December 2020. Note elevated turbidity in bottom photo.

collapse over the course of the study period (Fig. A16). There was also a large rootwad in the middle of the channel that degraded during the study, supplying sediment to the stream (Fig. A17).

Figure 8. BOG in Dec-20 indicating (A) treefall along the bank, (B) slumping, and (C) a mid-channel gravel bar. Blue arrow indicates flow direction.


Figure 9. View downstream from within the tributary to SWP showing channel incision and bank erosion in Dec-20.

4.4. Geomorphic Response

Bed-material mobilization in burned sites induced changes in bed grain size and local changes in channel geometry, although gross channel changes in width, depth, slope, and bed roughness height were limited (Table 4; Figs. 12 and 13). Peak flows in burned sites in WYs 2021 and 2022 were competent to transport the D_{50} at nearly all cross-sections. In MCR, flows were not competent to transport the D_{50}. Boulders were not mobilized during the study period (Table A10). Here, I provide my site-specific interpretation of morphologic change, based on field

observations and channel change calculations. I generalize these results across study sites and in the larger context of sediment inputs, flow competence, and instream wood in the Discussion.

Table 4. Summary of channel morphology change (Δ) in study reaches.

	Avg. BF Depth[a]	Avg. BF Width[a]	D_{50}[a]	Reach Slope	Bed Roughness Height
WRT					
Dec-20	0.94 m	7.7 m	–	0.048	0.20 m
Jun-21	0.68 m	6.9 m	54 mm	0.043	0.20 m
Mar-22	0.77 m	8.2 m	82 mm	0.043	0.26 m
Δ Dec-20 – Jun-21	-28%	-10%	–	-0.005	0 m
Δ Jun-21 – Mar-22	+13%	+19%	+52%*	0	+0.06 m
Δ Dec-20 – Mar-22	-18%	+6%	–	-0.005	+0.06 m
BOG					
Dec-20	0.59 m	5.9 m	23 mm	0.060	0.26 m
Jun-21	0.60 m	6.1 m	24 mm	0.060	0.25 m
Mar-22	0.61 m	5.3 m	36 mm	0.059	0.21 m
Δ Dec-20 – Jun-21	+1.7%	+3%	+4.2%	0	-0.01 m
Δ Jun-21 – Mar-22	+1.7%	-13%	+50%	-0.001	-0.04 m
Δ Dec-20 – Mar-22	+3.4%	-10%	+57%*	-0.001	-0.05 m
SWP					
Dec-20	0.48 m	2.4 m	3 mm	0.100	0.28 m
Jun-21	0.51 m	2.4 m	10 mm	0.097	0.23 m
Mar-22	0.64 m	2.4 m	12 mm	0.097	0.29 m
Δ Dec-20 – Jun-21	+6%	0%	+230%*	-0.003	-0.05 m
Δ Jun-21 – Mar-22	+25%	0%	+20%	0	+0.06 m
Δ Dec-20 – Mar-22	+33%	0%	+300%*	-0.003	+0.01 m
CON					
Dec-20	0.52 m	9.0 m	28 mm	0.059	0.24 m
Jun-21	0.57 m	9.0 m	52 mm	0.056	0.21 m
Mar-22	0.76 m	9.2 m	47 mm	0.057	0.19 m
Δ Dec-20 – Jun-21	+10%	+0%	+86%*	-0.003	-0.03 m
Δ Jun-21 – Mar-22	+33%	+2%	-10%	+0.001	-0.02 m
Δ Dec-20 – Mar-22	+46%	+2%	+68%*	-0.002	-0.05 m
MCR[b]					
Aug-19	0.34 m	4.7 m	90 mm	0.058	0.227 m
Jun-21	0.36 m	4.5 m	56 mm	0.062	0.199 m
Δ Aug-19 – Jun-21	+6%	-4%	-38%	+0.004	-0.028 m

[a] Statistical differences in populations indicated by * ($P < 0.05$).

[b] Change in BF depth, BF width, and D_{50} calculated at a single repeat cross-section, not the reach. As such, statistical testing was not performed for depth and width changes.

4.4.1. Wright Creek

There were no obvious post-fire effects on channel morphology in WRT during initial surveys 1.5 months after the fires. The only significant change was during the second winter rainy season after the fires, when there was significant coarsening of the bed material and the D_{50} increased by 52% (Table 4; Fig. 13). Bed material immediately upstream of a large wood jam was significantly finer than downstream (Fig. 13). Although there were no significant changes in average bankfull depth (Table 4), repeat longitudinal profiles suggest there was substantial erosion in the upper portion of the reach during the study (Fig. 12).

4.4.2. Bogus Creek

1.5 months after the fires, there was notable gravel aggradation in BOG that appeared to be post-fire deposition (Figs. 8, 10, and A15). The gravel mostly persisted during the first winter after the fires, and further aggraded in some areas (Fig. 10), but was largely eroded during the second winter rainy season (Figs. 10 and A18). This is supported by repeat pebble counts which showed little change in the D_{50} during the first winter and a 50% increase during the second winter (Table 4; Fig. 13), reflecting bed-material coarsening. Only the change in grain size distribution between Dec-20 and Mar-22 was statistically significant (Fig. 13).

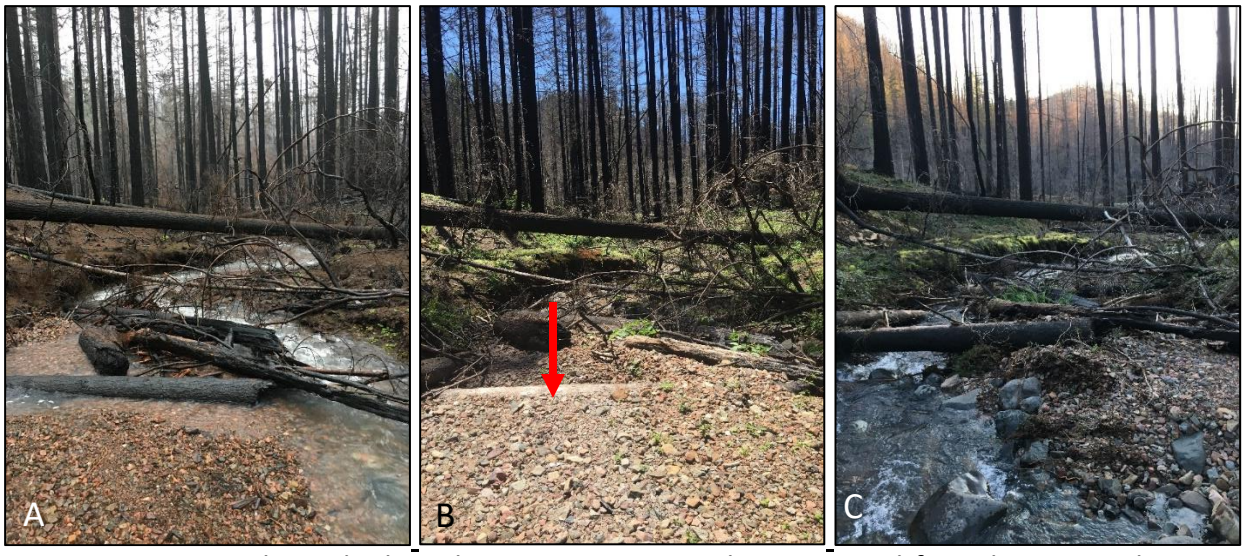

Figure 10. Repeat photos looking downstream in BOG showing wood-forced coarse sediment aggradation between (A) Dec-20 and (B) Jun-21 and erosion by (C) Mar-22. Between (B) and (C) there was >0.6 m of channel incision at the location indicated by the arrow in (B).

4.4.3. Swamp Creek

SWP is the steepest study reach, and exhibited the most defined step-pool system, with large steps composed of boulders and organic debris. The D_{50} (excluding step-forming boulders) was 3 mm 1.5 months after the fires (Table 4), suggesting that steps trapped a substantial amount of fine sediment in pools. Although not statistically significant, there was a 32% increase (+0.16

m) in average bankfull depth during the study (Table 4). This, in conjunction with significant bed-material coarsening (Table 4; Fig. 13), suggests there was flushing of fine sediments over the study period that resulted in channel degradation.

4.4.4. Cone Creek

There was a marginal channel bar of fine to cobble-sized sediment at the downstream end of CON 1.5 months after the fires that appeared to be post-fire deposition. During the first winter rainy season after the fires, the marginal bar began to erode, and a new mid-channel bar formed (Fig. 11). There was also substantial gravel deposition above large wood jams at the upstream and downstream ends of the reach during the initial rainy season (Fig. A19). While

Fig. 11. Repeat photos looking upstream in CON showing mid-channel bar formation between (A) Dec-20 and (B) Jun-21 and erosion by (C) Mar-22. Note bank erosion and widening of the bankfull channel at left in (C).

the jam-forced gravel deposition persisted through the second rainy season (Fig. A19), flows eroded the newly formed mid-channel bar and cut into the bank, widening the bankfull channel (Fig. 11). This erosion was accompanied by an increase in average bankfull depth of 33% (+0.19 m), although this was not statistically significant (Table 4). Bed material coarsened significantly during the initial winter, and then remained consistent (Table 4; Fig. 13).

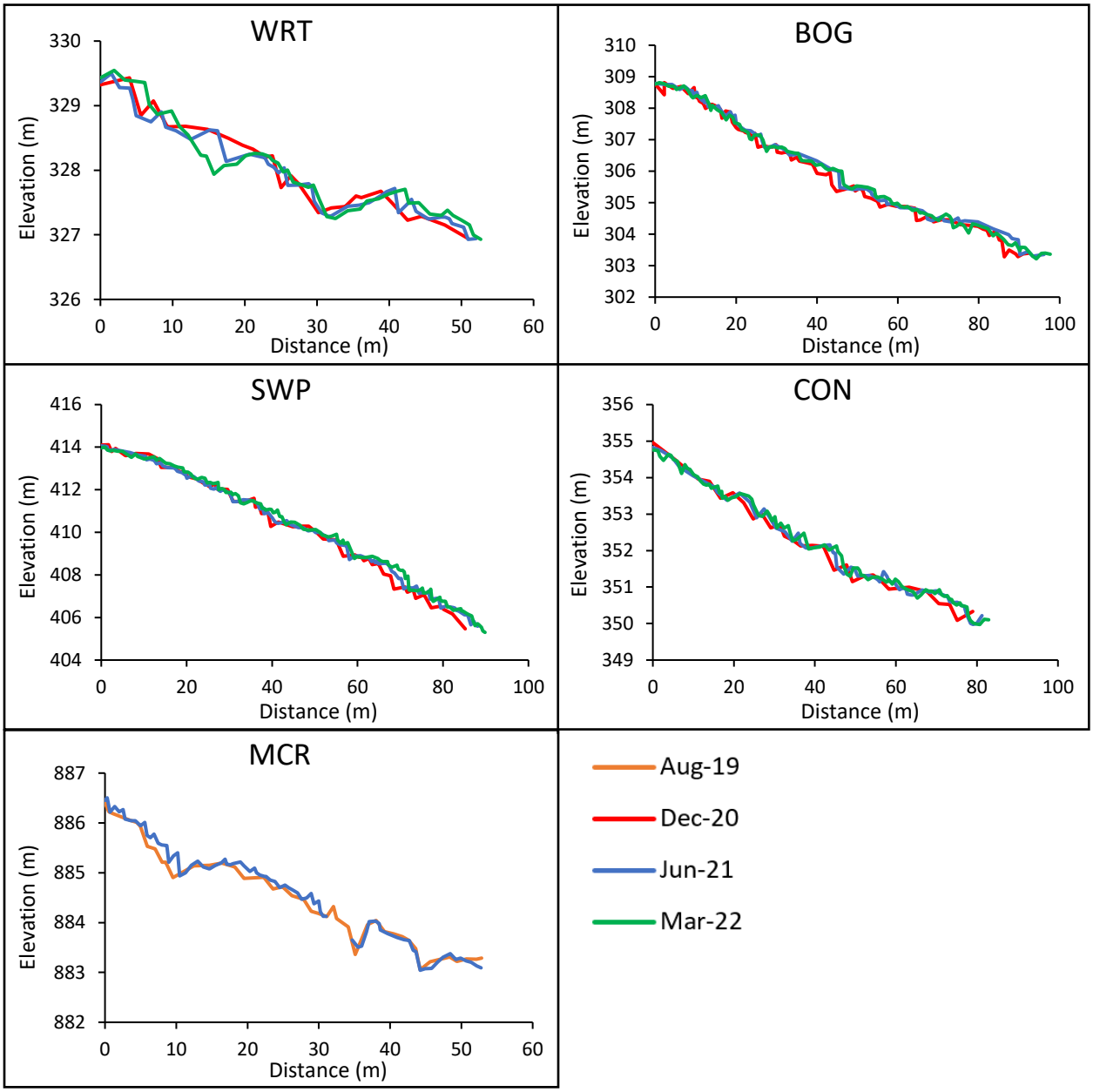

Figure 12. Thalweg longitudinal profiles of study reaches. Changes were mostly minor, but note degradation in the upper portion of WRT over the course of the study. Because the thalweg location sometimes shifted between surveys, plots may not accurately depict areas of incision and deposition. Axes scaled to data.

4.4.5. McRae Creek

MCR appeared to be morphologically stable from August 2019 to June 2021. Time-lapse photos showed little change in channel morphology at the trail camera location between 2019 and 2021, although some mobilization of large cobbles was evident. Changes in grain size distribution were not significant, although the D_{50} decreased by 38% during the two-year period (Table 4; Fig. 13).

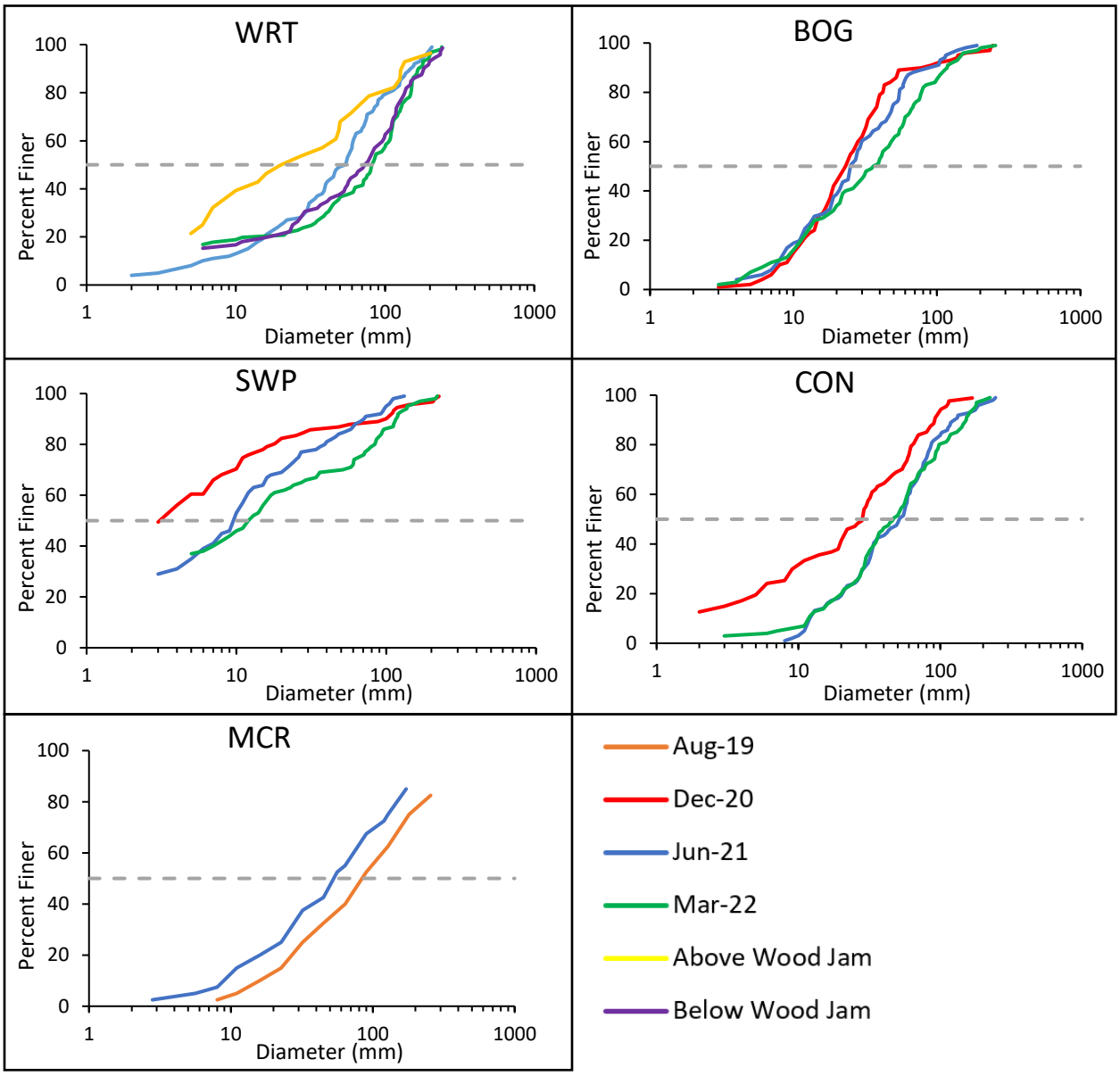

Figure 13. Grain size distributions in study reaches. There were statistically significant changes in grain size between Dec-20 and Jun-21 in SWP and CON, between Jun-21 and Mar-22 in WRT, and between Dec-20 and Mar-22 in BOG, SWP, and CON. Differences in grain size above and below a large wood jam in WRT were also significant. Gray dashed line indicates D_{50}.

4.5. Instream Wood

There was abundant burned downed woody debris on hillslopes and in the riparian area adjacent to burned study sites. The quantity of instream large wood did not appear to change substantially during the study period, although I noted additional treefall in WRT and SWP following the first winter rainy season after the fires (Fig. A20). There was between 10.3 and 18.3 pieces of large wood per 100 m stream length in burned sites (Table A18). 85% of pieces were partially or completely burned (Table A19). I assumed large wood pieces that were both burned and mostly covered in bark were post-fire additions to the stream channel. By this assumption, 34% of total pieces were recruited to channels after the fires. 60% of these pieces appeared to be sourced from the riparian area or adjacent hillslopes and formed bridges or ramps, reflecting post-fire treefall. 29% of large wood pieces formed channel-spanning jams in WRT, SWP, and CON. 14% of pieces were contributing to sediment aggradation and the formation of bars (Table A19). There was an average of 36% less instream wood pieces in my unburned site, MCR, then in burned sites (Table A18). All pieces were deteriorated and did not appear to be recently recruited to the channel. 40% of pieces were contributing to bar formation (Table A19). In all sites, there was abundant wood <20 cm in diameter that persisted over the study period.

5. Discussion

5.1. Hydrologic Response

In the 1.5 years after the wildfires, peak flows in burned sites remained mostly confined to the bankfull channel and did not exceed the two-year recurrence interval flood (Table 3). Peak unit discharges were often lower in smaller burned catchments than in larger unburned catchments (Tables 3, A7, and A8). This is the opposite of what would be expected. One explanation is that I underestimated peak discharges in burned sites, which were ungaged. These trends may also be attributed to below-average precipitation during the study period (Table 2) and the high infiltration capacity of soils in the region, which may have dampened fire-induced increases in runoff. Erosive overland flow only occurred during a few storms exceeding a 24-hour, ~1.6 mm hr^{-1} intensity. This is consistent with previous studies in the region suggesting high infiltration capacities even after wildfire (Wondzell and King, 2003). Some variability in timing and magnitude of peak flows among nearby sites suggests there was variability in precipitation that was not captured by available rain gage data. The highest peak-flow recurrence interval estimated here (~5 years, WY 2021; Table 3) was in MCR, the unburned reference reach, highlighting the influence of other processes besides wildfire (e.g., rain-on-snow events) in driving variations in flow across catchments.

5.2. Geomorphic Response

In the 1.5 years after the fires, burned sites exhibited changes in bed-material size and local changes in channel geometry from aggradation and erosion, although changes in gross channel form were limited. Observations indicate burned sites were in sediment transport-limited

conditions in the first winter rainy season after the fires, contrary to the typical supply-limited conditions inherent to steep streams. Transport-limited conditions resulted from the combination of a post-fire sediment pulse and post-fire recruitment of large wood. The sediment pulse was derived from slumping, sheetwash, and minor bank erosion. After the wildfires, the amount of large wood pieces in burned sites increased by ~50%, which increased flow resistance and reduced transport capacity. This resulted in the accumulation of fine to cobble-sized sediment in channels, which decreased bed grain size and lowered the threshold for motion of the median clast. During the second winter after the fires, streams evolved toward supply-limited conditions. Peak flows exceeded critical shear stress for mobilization of the D_{50}, leading to significant coarsening of channel bed material and minor channel degradation. This pattern applies even in WRT, where two landslides upstream of my reach in January 2022 increased sediment supply. While there was a notable spike in turbidity following the landslides (Fig. A11), I posit that coarser sediment delivered to the channel had not yet been transported to my reach, perhaps due to reduced transport capacity associated with post-fire wood loading.

These results contrast those in my unburned reference reach, where there were no recent additions of large wood, peak flows were not competent to transport the median grain size, and there were no significant changes in bed-material size between 2019 and 2021, despite a ~5-year recurrence interval flood in 2021. The post-fire sediment pulse, recruitment of large wood, and resultant sequence of channel aggradation followed by erosion in burned sites are consistent with previous studies of steep stream response to wildfire (e.g., Florsheim et al., 1991; Keller et al., 1997; Minshall et al., 1997). Observations of substantial sediment stored by wood in BOG and CON (Figs. 10, A18, and A19) reinforce those found by Wohl et al. (2022), suggesting that instream wood plays an import role in attenuating downstream sediment pulses after wildfire.

5.3. Controls on Channel Response

Here, I examine potential controls on the observed hydrogeomorphic responses, considering the tiered controls on stream response to wildfire shown in Figure 2. The high burn severity of the 2020 fires, steep topography, and high mean annual precipitation of study sites (Table 1) suggested that these streams would be highly susceptible to geomorphic change from post-fire flooding and debris flows. This was not the case during the study period, suggesting that thresholds were not exceeded, either to trigger debris flows or to mobilize large clasts and initiate widespread channel change.

Flooding and debris flows in mountain watersheds are driven by heavy precipitation (e.g., Pitlick, 1994; Jakob and Hungr, 2005). An analysis of 15-minute and 24-hour precipitation thresholds for landslides and debris flows in Western Oregon (details provided in the Appendix) indicates that thresholds were not exceeded during the study period. In WRT, which had the greatest density of roads (Table 1), the combined effects of wildfire and road development lowered precipitation thresholds, triggering two landslides. Below-average precipitation during the study period (Z-scores of -0.57 to -1.7; Table 2), combined with the absence of threshold-

exceeding events, likely explain relatively minor hydrogeomorphic responses, by limiting channel-restructuring floods and debris flows. This is consistent with previous studies indicating post-fire precipitation has a strong influence on channel response to wildfire (e.g., Chin et al., 2019; Brogan et al., 2019).

Subtle variations in geomorphic responses among sites reflect differences in the balance of sediment supply to transport capacity. For example, substantial coarse sediment aggradation in BOG and CON is suggestive of greater inputs of sediment and/or lower transport capacity in these sites. Variations in climatic and biophysiographic characteristics among study sites (Table 1) highlight the complex interactions of factors that drive these differences. For instance, the combination of steep basin slopes and high burn severity in BOG and CON (Table 1) may have contributed to greater hillslope erosion and sediment inputs to streams. Alternatively, the steep gradient of SWP (Table 1) may have increased transport capacity relative to other sites. To further understand the controls on variable stream responses to wildfire, there is a need for long-term investigations across many sites spanning climatic and biophysiographic gradients.

5.4. The Role of Climate Change

The extreme fuel aridity that in part drove the severe 2020 wildfires in the Western Cascades (Abatzoglou et al., 2021) was consistent with an extended drought across much of the western United States, including Oregon, since the year 2000 (Williams et al., 2022). Both the extended drought (through WY 2021) and increased fuel aridity in recent decades have been attributed to human-induced climate change (Williams et al., 2022; Abatzoglou and Williams, 2016). The drought in Oregon continued into WY 2022, as evidenced by below-average precipitation in the study area (Table 2). Anthropogenic climate change may thus have not only contributed to the severity of the 2020 wildfires, but also influenced the muted responses in my study streams, by contributing to continued below-average precipitation. Drought following severe wildfire may also slow vegetation recovery or result in the conversion of pre-fire forest to non-forest vegetation (Coop et al., 2020). This may prolong the period in which post-fire landslides and debris flows may occur, by delaying or preventing reestablishment of root systems and associated stabilization of hillslopes (Hatchett et al, 2021). Further, intense precipitation events in western Oregon are projected to increase in frequency in response to climate change (e.g., Cooley and Chang, 2021), which would produce greater susceptibility to post-fire flooding and debris flows in the future. Climate change may thus have complex, multifaceted effects on post-fire landscape response, in a manner that challenges current predictive capacities. Further work is needed to assess the impacts of a changing climate on mountain watershed response to wildfire in western Oregon, to guide post-fire land management decisions.

5.5. Challenges, Implications, and Future Outlook

This study exemplifies the challenges of assessing mountain stream response to wildfire. First, pre-fire channel morphology data are rarely available, and it is often difficult and dangerous to access burned areas immediately following fire, before changes occur. This was the case in this study, where rainstorms in mid-November 2020, before my initial survey, very likely altered

pre-fire conditions in study reaches. Second, reach-scale studies may not capture diverse geomorphic responses across watersheds, an example being the occurrence of two landslides upstream of my study reach in WRT. Finally, this study highlights the importance of timescales when considering stream responses to wildfire. Short-term studies are inherently limited because some landscape responses to disturbance may not manifest for months to decades. For example, in the two months after the landslides in WRT, coarse sediment had not yet been transported to my reach, temporarily limiting the effects of the slides on channel morphology in my reach. Additionally, in the immediate years after fire, root systems of burned vegetation may persist, temporarily adding cohesion and associated hillslope stability until root-system decay (Shakesby and Doerr, 2006). Further, periods of below-average precipitation coupled with an absence of extreme precipitation events may temporarily limit runoff and erosion responses, as was the case in this study. To improve understanding of landscape response to fire, especially considering the uncertain effects of climate change, there is a need for research examining responses at greater spatial and temporal scales. Approaches such as repeat airborne laser scanning (e.g., Brogan et al., 2019) are better suited for this than traditional total station surveys, but may be prohibitively expensive.

Impacts of post-fire runoff and erosion on stream ecosystems is a primary concern of post-fire hazard assessment teams (e.g., FEMA, 2020; BAER, 2020). In the 1.5 years after the fires, post-fire recruitment of large wood will likely have the most prolonged effect on habitat by creating roughness, reducing transport capacity, and mediating downstream sediment delivery (e.g., Montgomery et al., 2003). This may be beneficial to stream biota by increasing habitat complexity (e.g., Fausch and Northcote, 1992). Increases in turbidity and fine sediment accumulation in channels may be deleterious to aquatic habitat (Wood and Armitage, 1997) and represent a short-term threat to spawning success for salmonids and lamprey (FEMA, 2020). Further, coarse sediment aggradation can cause summer base flows to drop below the level of the bed, creating discontinuities in the wetted channel and reducing pool capacity (May and Lee, 2004). Although I did not observe this in study sites, coarse sediment aggradation in BOG and CON caused marked reductions in wetted channel area following the first winter after the fires (Figs. 10, A18, and A19). The onset of channel incision and flushing of fine sediments in the second winter after the fires suggests study sites are on a trajectory of recovery to pre-fire bed-material conditions. Effects on the larger North Umpqua and McKenzie river systems and fisheries were likely minor in the 1.5 years after the fires, due to the absence of significant flooding and debris flows.

Future precipitation that exceeds thresholds for flooding and debris flows could trigger widespread destabilization in study sites and subsequent flooding of downstream areas with water and sediment. Alternatively, steep streams may prove resilient to destabilization even during large floods, and high transport capacities may be sufficient to flush large inputs of sediment without compromising channel bed structure. Road fill failure represents a persistent risk in the study area, as illustrated by road-induced landslides in WRT during an unexceptional storm (1-day, 49 mm; Table 2). Fill failure in locations with other enabling conditions (Benda and Cundy, 1990) could trigger debris flows in streams. Salvage logging and hazard tree removal operations in the study area may also influence post-fire landscape changes. In addition to

removing large wood from the landscape that provides ecosystem functions and that may otherwise be recruited to stream channels and modulate downstream sediment transport, this may increase hillslope runoff and erosion rates, although increases depend strongly on site characteristics and logging methods (McIver and Starr, 2001). Ultimately, continued monitoring in a manner consistent with this work or, ideally, at greater spatial scales, will be necessary to fully understand the impacts of the severe 2020 wildfires on steep mountain streams of the Western Cascades.

6. Conclusion

Changes in fluxes of water, sediment, and large wood in the 1.5 years after severe wildfire in the Western Cascades induced an evolving balance of sediment supply to transport capacity in steep streams. Bed-material size exhibited the greatest susceptibility to change, while gross channel form showed resilience, despite local aggradation and erosion. Post-fire inputs of large wood will have prolonged implications for channel morphology and habitat heterogeneity. Anthropogenic climate change, which likely contributed to below-average precipitation during the study, may exert a complex influence on channel response to wildfire in Western Oregon by lowering total precipitation while simultaneously increasing the frequency of extreme rain events and the duration in which these events may trigger flooding and debris flows.

References

Abatzoglou, J.T., Rupp, D.E., O'Neill, L.W., and Sadegh, M., 2021, Compound Extremes Drive the Western Oregon Wildfires of September 2020: Geophysical Research Letters, v. 48, p. 1–9, doi:10.1029/2021GL092520.

Abatzoglou, J.T., and Williams, A.P., 2016, Impact of anthropogenic climate change on wildfire across western US forests: Proceedings of the National Academy of Sciences of the United States of America, v. 113, p. 11770–11775, doi:10.1073/pnas.1607171113.

Benda, L., 1990, The influence of debris flows on channels and valley floors in the Oregon Coast Range, U.S.A.: Earth Surface Processes and Landforms, v. 15, p. 457–466, doi:10.1002/esp.3290150508.

Benda, L.E., and Cundy, T.W., 1990, Predicting deposition of debris flows in mountain channels: Canadian Geotechnical Journal, v. 27, p. 409–417, doi:10.1139/t90-057.

Benda, L., and Dunne, T., 1997, Stochastic forcing of sediment supply to channel networks from landsliding and debris flow: Water Resources Research, v. 33, p. 2849–2863, doi:10.1029/97WR02388.

Benda, L., Miller, D., Bigelow, P., and Andras, K., 2003b, Effects of post-wildfire erosion on channel environments, Boise River, Idaho: Forest Ecology and Management, v. 178, p. 105–119, doi:10.1016/S0378-1127(03)00056-2.

Benda, L., Veldhuisen, C., and Black, J., 2003a, Debris flows as agents of morphological heterogeneity at low-order confluences, Olympic Mountains, Washington: Bulletin of the Geological Society of America, v. 115, p. 1110–1121, doi:10.1130/B25265.1.

Bigelow, P.E., Benda, L.E., Miller, D.J., and Burnett, K.M., 2007, On Debris Flows, River Networks, and the Spatial Structure of Channel Morphology: Forest Science, v. 53, p. 220–238, doi:10.1093/forestscience/53.2.220.

Brogan, D.J., Nelson, P.A., and MacDonald, L.H., 2019, Spatial and temporal patterns of sediment storage and erosion following a wildfire and extreme flood: Earth Surface Dynamics, v. 7, p. 563–590, doi:10.5194/esurf-7-563-2019.

Carroll, S., 2021, Insurance companies sue Pacific Power over Archie Creek Fire: The News-Review.

Cerda, A., and Doerr, S.H., 2005, Influence of vegetation recovery on soil hydrology and erodibility following fire: an 11-year investigation: International Journal of Wildland Fire, p. 423–437, doi:10.1071/WF05044.

Chin, A., Solverson, A.P., O'Dowd, A.P., Florsheim, J.L., Kinoshita, A.M., Nourbakhshbeidokhti, S., Sellers, S.M., Tyner, L., and Gidley, R., 2019, Interacting geomorphic and ecological response of step-pool streams after wildfire: GSA Bulletin, v. 131, p. 1480–1500, doi:10.1130/B35049.1.

Church, M., 2006, Bed Material Transport and the Morphology of Alluvial River Channels: Annual Review of Earth and Planetary Science, v. 34, p. 325–356, doi:10.1146/annurev.earth.33.092203.122721.

Coleman, S.E., Nikora, V.I., and Aberle, J., 2011, Interpretation of alluvial beds through bed-elevation distribution moments: Water Resources Research, v. 47, p. 1–14, doi:10.1029/2011WR010672.

Comiti, F., and Mao, L., 2012, Recent Advances in the Dynamics of Steep Channels: Gravel-Bed Rivers: Processes, Tools, Environments, p. 351–377, doi:10.1002/9781119952497.ch26.

Conrey, R.M., Sherrod, D.R., Donnelly-Nolan, J.M., and Taylor, E.M., 2002, The North-Central Oregon Cascade Margin: Exploring Petrologic and Tectonic Intimacy in a Propagating Intra-Arc Rift, *in* Field Guide to Geologic Processes in Cascadia: Oregon Department of Geology and Mineral Industries Special Paper 26, p. 47–90.

Cooley, A.K., and Chang, H., 2021, Detecting change in precipitation indices using observed (1977–2016) and modeled future climate data in Portland, Oregon, USA: Journal of Water and Climate Change, v. 12, p. 1135–1153, doi:10.2166/wcc.2020.043.

Coop, J.D., Parks, S.A., Stevens-Rumann, C.S., Crausbay S.D., Higuera, P.E., Hurteau, M.D., Tepley, A., Whitman, E., Assal, T., Collins, B.M., Davis, K.T., Dobrowski, S., Falk, D.A., Fornwalt, P.J., Fule, P.Z., Harvey, B.J., Kane, V.R., Littlefield, C.E., Margolis, E.Q., North, M., Parisien, M., Prichard, S., Rodman, K.C., 2020, Wildfire-Driven Forest Conversion in Western North American Landscapes: BioScience, v. 70, p. 659–673, doi:10.1093/biosci/biaa061.

Fausch, K.D., and Northcote, T.G., 1992, Large woody debris and salmonid habitat in a small coastal British Columbia stream: Canadian Journal of Fisheries and Aquatic Sciences, v. 49, p. 682–693, doi:10.1139/f92-077.

Federal Emergency Management Agency (FEMA), 2020, Archie Creek Fire Erosion Threat Assessment/Reduction Team (ETART) Summary Report: https://gscdn.govshare.site/1aa8ace4addf06592a8d7dcb775413bf10fd1ec6/ETARTSummary-ArchieFire.pdf

Florsheim, J.L., Chin, A., Kinoshita, A.M., and Nourbakhshbeidokhti, S., 2017, Effect of storms during drought on post-wildfire recovery of channel sediment dynamics and habitat in the southern California chaparral, USA: Earth Surface Processes and Landforms, v. 42, p. 1482–1492, doi:10.1002/esp.4117.

Florsheim, J.L., Keller, E.A., and Best, D.W., 1991, Fluvial sediment transport in response to moderate storm flows following chaparral wildfire, Ventura County, southern California: Geological Society of America Bulletin, v. 103, p. 504–511, doi:10.1130/0016-7606(1991)103<0504:FSTIRT>2.3.CO;2.

Germanoski, D., and Miller, J.R., 1995, Geomorphic response to wildfire in an arid watershed, Crow Canyon, Nevada: Physical Geography, v. 16, p. 243–256, doi:10.1080/02723646.1995.10642552.

Grant, G.E., Swanson, F.J., and Wolman, M.G., 1990, Pattern and origin of stepped-bed morphology in high-gradient streams, Western Cascades, Oregon: GSA Bulletin, v. 102, p. 340–352, doi:10.1130/0016-7606(1990)102<0340:PAOOSB>2.3.CO;2.

Halofsky, J.E., Peterson, D.L., and Harvey, B.J., 2020, Changing wildfire, changing forests: the effects of climate change on fire regimes and vegetation in the Pacific Northwest, USA: Fire Ecology, v. 16, doi:10.1186/s42408-019-0062-8.

Hatchett, B., McGuire, L., Youberg, A., Hoch, O., Oakley, N., McEvoy, D., Albano, C., and Lancaster, J., The role of drought in the persistence of post-fire hydrologic hazards: Abstract H53G-06 presented at 2021 Fall Meeting, AGU, New Orleans, LA, 13-17 December.

Hoffman, D.F., and Gabet, E.J., 2007, Effects of sediment pulses on channel morphology in a gravel-bed river: GSA Bulletin, v. 119, p. 116–125, doi:10.1130/B25982.1.

Jackson, M., and Roering, J.J., 2009, Post-fire geomorphic response in steep, forested landscapes: Oregon Coast Range, USA: Quaternary Science Reviews, v. 28, p. 1131–1146, doi:10.1016/j.quascirev.2008.05.003.

Jakob, M., and Hungr, O., 2005, Debris-flow hazards and related phenomena: Berlin, Germany, Springer, 739 p.

Jefferson, A., Grant, G.E., Lewis, S.L., and Lancaster, S.T., 2010, Coevolution of hydrology and topography on a basalt landscape in the Oregon Cascade Range, USA: Earth Surface Processes and Landforms, v. 35, p. 803–816, doi:10.1002/esp.1976.

Kavanaugh, S.D., and Sickinger, T., 2020, Explosion, sparks from power line preceded Oregon's Holiday Farm fire, area residents say: The Oregonian.

Keller, E.A., Valentine, D.W., and Gibbs, D.R., 1997, Hydrological response of small watersheds following the Southern California painted cave fire of June 1990: Hydrological Processes, v. 11, p. 401–414, doi:10.1002/(sici)1099-1085(19970330)11:4<401::aid-hyp447>3.0.co;2-p.

Littell, J.S., McKenzie, D., Wan, H.Y., and Cushman, S.A., 2018, Climate Change and Future Wildfire in the Western United States: An Ecological Approach to Nonstationarity: Earth's Future, v. 6, p. 1097–1111, doi:10.1029/2018EF000878.

May, C.L., and Lee, D.C., 2004, The Relationships among In-Channel Sediment Storage, Pool Depth, and Summer Survival of Juvenile Salmonids in Oregon Coast Range Streams: North American Journal of Fisheries Management, v. 24, p. 761–774, doi:10.1577/m03-073.1.

McIver, J.D., and Starr, L., 2001, A literature review on the environmental effects of postfire logging: Western Journal of Applied Forestry, v. 16, p. 159–168, doi:10.1093/wjaf/16.4.159.

McNabb, D., and Swanson, F., 1990, Effects of Fire on Soil Erosion: Journal of Range Management, v. 46, p. 470, doi:10.2307/4002670.

Meyer, G.A., and Wells, S.G., 1997, Fire-related sedimentation events on alluvial fans, Yellowstone National Park, U.S.A.: Journal of Sedimentary Research, v. 67, p. 776–791, doi:10.1306/d426863a-2b26-11d7-8648000102c1865d.

Minshall, G.W., Robinson, C.T., and Lawrence, D.E., 1997, Postfire responses of lotic ecosystems in Yellowstone National Park, U.S.A: Canadian Journal of Fisheries and Aquatic Sciences, v. 54, p. 2509–2525, doi:10.1139/cjfas-54-11-2509.

Montgomery, D.R., and Buffington, J.M., 1997, Channel-reach morphology in mountain drainage basins: GSA Bulletin, v. 109, p. 596–611, doi:10.1130/0016-7606(1997)109<0596:CRMIMD>2.3.CO;2.

Montgomery, D.R., and Buffington, J.M., 1998, Channel Processes, Classification, and Response: River Ecology and Management, p. 13–42, doi:10.1007/978-1-4612-1652-0_2.

Montgomery, D.R., Collins, B.D., Buffington, J.M., and Abbe, T.B., 2003, Geomorphic effects of wood in rivers: American Fisheries Society Symposium, v. 37, p. 21–47.

Moody, J.A., and Martin, D.A., 2009, Synthesis of sediment yields after wildland fire in different rainfall regimes in the western United States: International Journal of Wildland Fire, v. 18, p. 96–115, doi:10.1071/WF07162.

Moody, J.A., Shakesby, R.A., Robichaud, P.R., Cannon, S.H., and Martin, D.A., 2013, Current research issues related to post-wildfire runoff and erosion processes: Earth-Science Reviews, v. 122, p. 10–37, doi:10.1016/j.earscirev.2013.03.004.

Neary, D.G., Gottfried, G.J., and Ffolliott, P.F., 2003, Post-Wildfire Watershed Flood Responses: Second International Fire Ecology and Fire Management Congress, Orlando, Florida, 16-20 November 2003, Paper 1B7, p. 1–8.

O'Connor, J.E., Mangano, J.F., Anderson, S.W., Wallick, J.R., Jones, K.L., and Keith, M.K., 2014, Geologic and physiographic controls on bed-material yield, transport, and channel morphology for alluvial and bedrock rivers, western Oregon: Bulletin of the Geological Society of America, v. 126, p. 377–397, doi:10.1130/B30831.1.

Pitlick, J., 1994, Relation between peak flows, precipitation, and physiography for five mountainous regions in the western USA: Journal of Hydrology, v. 158, p. 219–240, doi:10.1016/0022-1694(94)90055-8.

PRISM Climate Group (PRISM), 2022, 30-year normal precipitation, 1991-2020: https://prism.oregonstate.edu/normals/

Raymond, C.A., McGuire, L.A., Youberg, A.M., Staley, D.M., and Kean, J.W., 2020, Thresholds for post-wildfire debris flows: Insights from the Pinal Fire, Arizona, USA: v. 45, 1349–1360 p., doi:10.1002/esp.4805.

Recking, A., 2009, Theoretical development on the effects of changing flow hydraulics on incipient bed load motion: Water Resources Research, v. 45, p. 1–16, doi:10.1029/2008WR006826.

Recking, A., Leduc, P., Liébault, F., and Church, M., 2012, A field investigation of the influence of sediment supply on step-pool morphology and stability: Geomorphology, v. 139–140, p. 53–66, doi:10.1016/j.geomorph.2011.09.024.

Shakesby, R.A., and Doerr, S.H., 2006, Wildfire as a hydrological and geomorphological agent: Earth-Science Reviews, v. 74, p. 269–307, doi:10.1016/j.earscirev.2005.10.006.

Short, L.E., Gabet, E.J., and Hoffman, D.F., 2015, The role of large woody debris in modulating the dispersal of a post-fire sediment pulse: Geomorphology, v. 246, p. 351–358, doi:10.1016/j.geomorph.2015.06.031.

Sidle, R.C., Pearce, A.J., O'Loughlin, C.L., 1985, Hillslope Stability and Land Use: American Geophysical Union Water Resource Monograph no. 11, 140 p.

Staley, D.M., Negri, J.A., Kean, J.W., Laber, J.L., Tillery, A.C., and Youberg, A.M., 2017, Prediction of spatially explicit rainfall intensity–duration thresholds for post-fire debris-flow generation in the western United States: Geomorphology, v. 278, p. 149–162, doi:10.1016/j.geomorph.2016.10.019.

Swanson, F.J., 1981, Fire and geomorphic processes, *in* Mooney, H.A., Bonnicksen, T.M., Christiansen, N.L., Lotan, J.E., and Reiners, W.A., eds., Fire Regime and Ecosystem Properties, United States Department of Agriculture, Forest Service, General Technical Report WO vol. 26: Washington, DC, United States Government Planning Office, p. 401-421.

U.S. Department of Agriculture, Forest Service (USFS), 2022, FSGeodata Clearinghouse: https://data.fs.usda.gov/geodata/

U.S. Department of Interior, Geological Survey (USGS), 2020, Emergency Assessment of Post-Fire Debris-Flow Hazards: https://landslides.usgs.gov/hazards/postfire_debrisflow/

U.S. Department of Interior, Geological Survey (USGS), 2022a, Landscape Fire and Resource Management Planning Tools (LANDFIRE): https://landfire.gov/index.php

U.S. Department of Interior, Geological Survey (USGS), 2022b, StreamStats version 4: https://streamstats.usgs.gov/ss/

U.S. Department of Interior, Geology Survey, U.S. Department of Agriculture, Forest Service (USGS and USFS), 2020, BAER Imagery Support Program: https://burnseverity.cr.usgs.gov/baer/

U.S. Department of Interior, Geology Survey, U.S. Department of Agriculture, Forest Service (USGS and USFS), 2022, Monitoring Trends in Burn Severity: https://www.mtbs.gov/

Vieira, D.C.S., Fernández, C., Vega, J.A., and Keizer, J.J., 2015, Does soil burn severity affect the post-fire runoff and interrill erosion response? A review based on meta-analysis of field rainfall simulation data: Journal of Hydrology, v. 523, p. 452–464, doi:10.1016/j.jhydrol.2015.01.071.

Wall, S.A., Roering, J.J., and Rengers, F.K., 2020, Runoff-initiated post-fire debris flow Western Cascades, Oregon: Landslides, v. 17, p. 1649–1661, doi:10.1007/s10346-020-01376-9.

Wiley, T.J., 2000, Relationship between rainfall and debris flows in western Oregon: Oregon Geology, v. 62, p. 27–43.

Williams, A.P., Cook, B.I., and Smerdon, J.E., 2022, Rapid intensification of the emerging southwestern North American megadrought in 2020–2021: Nature Climate Change, v. 12, p. 232–234, doi:10.1038/s41558-022-01290-z.

Wohl, E., Cenderelli, D.A., Dwire, K.A., Ryan-Burkett, S.E., Young, M.K., and Fausch, K.D., 2010, Large in-stream wood studies: A call for common metrics: Earth Surface Processes and Landforms, v. 35, p. 618–625, doi:10.1002/esp.1966.

Wohl, E., Marshall, A.E., Scamardo, J., White, D., and Morrison, R.R., 2022, Biogeomorphic influences on river corridor resilience to wildfire disturbances in a mountain stream of the Southern Rockies, USA: Science of the Total Environment, v. 820, p. 153321, doi:10.1016/j.scitotenv.2022.153321.

Wolman, G.M., 1954, A Method of Sampling Course River-Bed Material: Transaction of the American Geophysical Union, v. 35, p. 951–956, doi:10.1029/TR035i006p00951.

Wolman, G.M., and Miller, J.P., 1960, Magnitude and Frequency of Forces in Geomorphic Processes: The Journal of Geology, v. 68, p. 54–74.

Wondzell, S.M., and King, J.G., 2003, Postfire erosional processes in the Pacific Northwest and Rocky Mountain regions: Forest Ecology and Management, v. 178, p. 75–87, doi:10.1016/S0378-1127(03)00054-9.

Wood, P.J., and Armitage, P.D., 1997, Biological effects of fine sediment in the lotic environment: Environmental Management, v. 21, p. 203–217, doi:10.1007/s002679900019.

Yochum, S.E., Comiti, F., Wohl, E., David, G.C.L., Mao, L., 2014, Photographic guidance for selecting flow resistance coefficients in high-gradient channels: U.S. Department of Agriculture, Forest Service, Rocky Mountain Research Station General Technical Report RMRS-GTR-323.

Appendix

Field Surveys

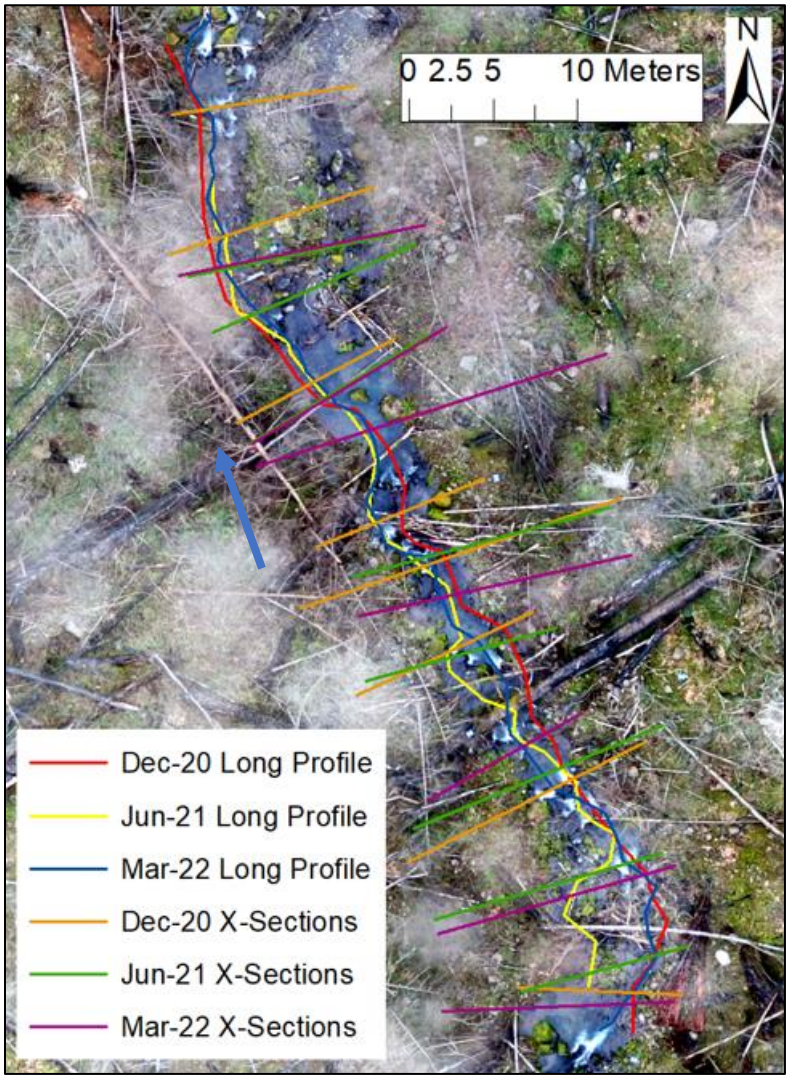

Figure A1. Long profile and cross-section survey locations in Wright Creek. Background is Mar-22 orthophoto. Blue arrow indicates flow direction.

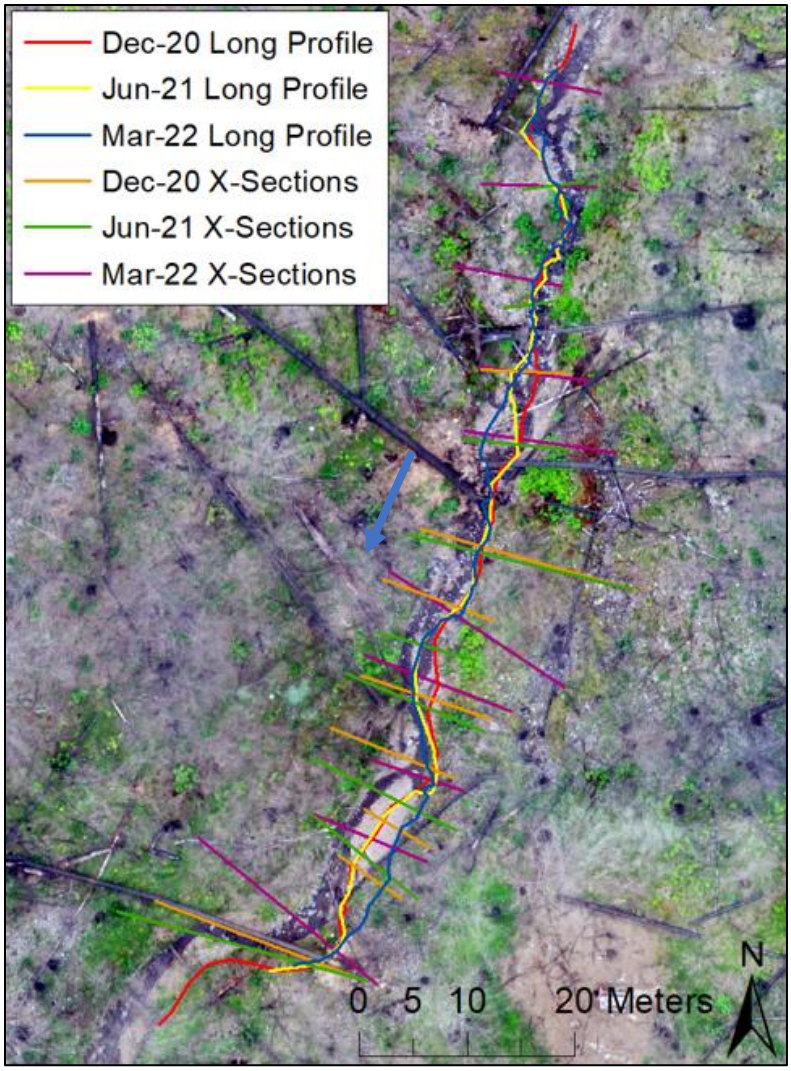

Figure A2. Long profile and cross-section survey locations in Bogus Creek. Background is Jun-21 orthophoto. Blue arrow indicates flow direction.

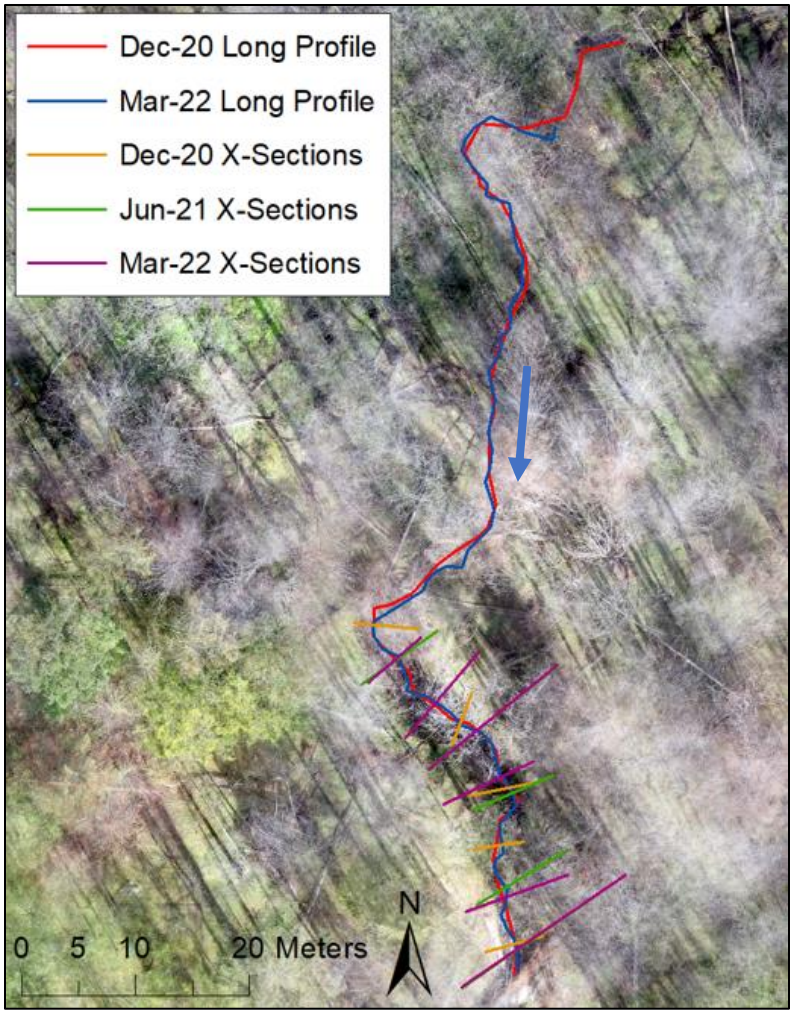

Figure A3. Long profile and cross-section survey locations in Swamp Creek. Long profile from Jun-21 is not included due to a transformation error. Background is Mar-22 orthophoto. Blue arrow indicates flow direction.

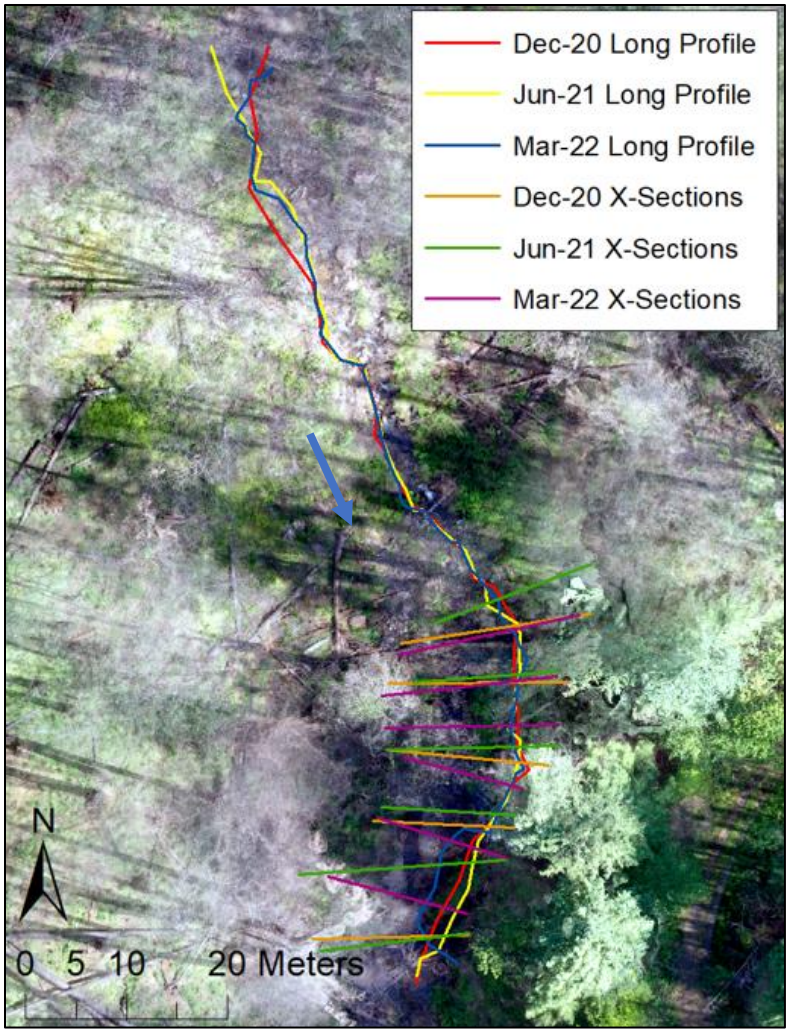

Figure A4. Long profile and cross-section survey locations in Cone Creek. Background is Jun-21 orthophoto. Blue arrow indicates flow direction.

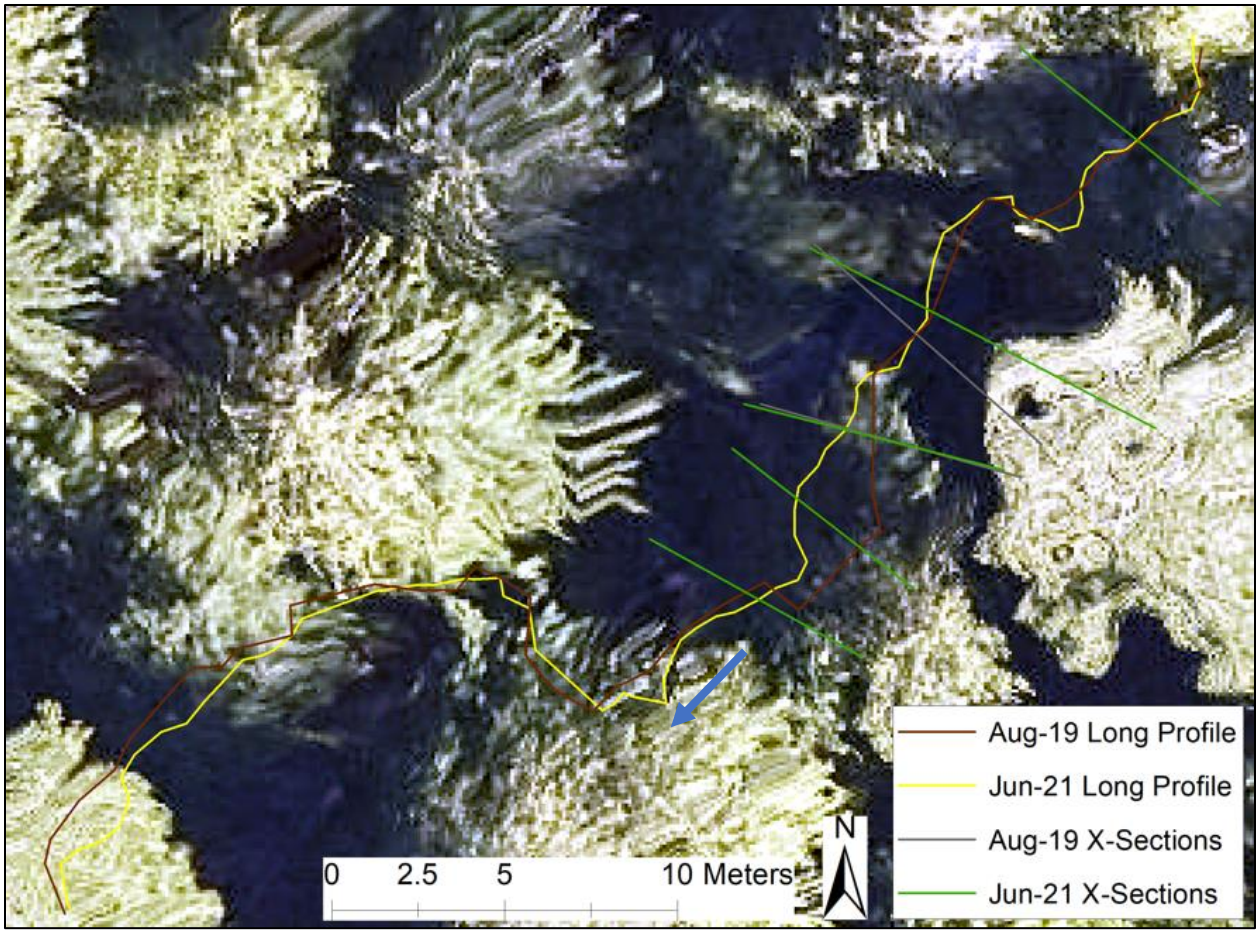

Figure A5. Long profile and cross-section survey locations in McRae Creek. August 2019 surveys were conducted by NEON staff. Background is July 2021 orthophoto completed by NEON. Blue arrow indicates flow direction.

McRae Creek Field Data Collection and Analyses

Because I only surveyed channel morphology in MCR in June 2021, I used data from a channel morphology survey conducted by NEON staff in August 2019 to evaluate change between 2019 and 2021, thereby approximating the two-winter period in which surveys were conducted in burned sites. NEON staff surveyed the thalweg elevation and two cross-sections in my study reach. I resurveyed one of these cross-sections, the discharge cross-section, in Jun-21, and calculated the percent change in bankfull width and depth at this single cross-section. As in my burned sites, I calculated the change in reach slope and bed roughness height. Due to different geographic transformations used between surveys, in order to perform the above calculations, I first aligned the two surveys in ArcGIS using permanent benchmarks that were surveyed in both August 2019 and June 2021. NEON staff also conducted a pebble count of 40 grains at the discharge cross-section using a gravelometer. I repeated this pebble count in Jun-21 and used these data for calculating the percent change in the D_{50} and testing for significant differences in grain size.

I did not survey the pressure transducer cross-section in MCR in Jun-21. As such, in order to evaluate peak flow stages, I used the cross-section geometry from the August 2019 survey. Given the minimal change in bankfull channel geometry between 2019 and 2021 at the repeat cross-section (Table 3), which is located 3.5 m downstream of the pressure transducer cross-section, I assumed that channel geometry from 2019 at the transducer was representative of current conditions. Because the datum for water surface elevation data differed from that used for surveying the transducer cross-section, I matched the water surface elevation surveyed in the field with the water surface elevation recorded by the pressure transducer near the time of the survey and adjusted all surveyed points by the difference.

HEC-RAS Modeling

I modeled peak-flow hydraulic conditions in WRT, BOG, and CON in HEC-RAS using cross-section geometries from Mar-22 field surveys. I did not model flows in SWP due to substantial flow being conveyed beneath undercut banks (Figs. 9 and A16). I interpolated cross-sections every 2–4 m depending on spacing of surveyed cross-sections. All simulations were run under a subcritical flow regime. I began by simulating the Mar-22 field discharge (Table A2) using known downstream water surface elevation as the boundary condition. I calibrated the model by varying Manning's n at each surveyed cross-section until the modeled water surface closely matched observed water surface. I did not vary Manning's n between the channel and overbank areas. Manning's n ranged from 0.05 to 0.3, which are typical values in mountain streams of similar geometry as my study streams (Yochum et al., 2014). Root mean squared error of the modeled water surface elevation for Mar-22 simulations was between 0.03 and 0.07 m (Table A1). To assess model performance at higher flows, I modeled the Dec-20 field discharge (Table A2) using normal depth as the boundary condition and compared modeled vs. observed water surface elevation at the pressure transducer, adjusting Manning's n as needed. I also compared modeled velocity near the discharge cross-section to observed velocity for both Dec-20 and Mar-22 simulations (Table A1). For my peak flow simulations (using normal depth boundary condition), I assumed Manning's n stayed constant at greater flows, and varied discharge until the modeled water surface at the transducer cross-section matched the observed water surface during the peak flow.

Table A1. Summary of HEC-RAS model validation and error assessment.

Site	Modeled Q	Validation Data Source	Model Error
WRT	Mar-22 field	Mar-22 observed WSE at all XS	RMSE = 0.07 m
		Mar-22 velocity at Q XS (XS3)	+11%
	Dec-20 field	Stage at pressure transducer (XS3)	+0.01 m
		Dec-20 velocity at Q XS (XS2)	-16%
BOG	Mar-22 field	Mar-22 observed WSE at all XS	RMSE = 0.03 m
		Mar-22 velocity at Q XS (XS3.4)	-5.3%
	Dec-20 field	Stage at pressure transducer (XS11)	+0.10 m
		Dec-20 velocity at Q XS (XS11)	-25%
CON	Mar-22 field	Mar-22 observed WSE at all XS	RMSE = 0.07 m
		Mar-22 velocity at Q XS (XS1.25)	-10%

	Dec-20 field	Stage at pressure transducer (XS4)	+0.07 m
		Dec-20 velocity at Q XS (XS1.5)	-47%

Table A2. Select at-a-station hydraulic metrics from HEC-RAS modeling of peak discharges in WYs 2021 and 2022. Data for interpolated cross-sections are not included.

Site	Water Year	XS[a]	EG Slope[b]	Channel Velocity (m/s)	Flow Area (m^2)	Top Width (m)	Max Depth (m)	Shear (N/m^2)
WRT	2021	1	0.037	0.29	3.11	12.94	0.45	83.55
		2	0.030	0.31	0.29	7.13	0.72	113.29
		3	0.011	0.33	2.76	7.90	0.74	34.77
		4	0.053	0.47	1.90	7.09	0.45	137.70
		5	0.073	0.42	2.16	6.33	0.59	225.50
		7	0.056	0.36	2.49	7.70	0.49	170.26
		8	0.049	0.37	2.45	6.39	0.54	168.93
	2022	1	0.037	0.32	4.00	13.94	0.51	99.47
		2	0.033	0.35	3.55	7.54	0.81	143.85
		3	0.012	0.37	3.53	8.93	0.83	42.55
		4	0.055	0.53	2.44	7.88	0.52	165.35
		5	0.082	0.46	2.80	7.59	0.68	272.97
		7	0.056	0.41	3.12	7.87	0.57	207.81
		8	0.050	0.42	3.10	6.73	0.64	207.08
BOG	2021	1	0.060	0.34	1.49	4.76	0.61	155.42
		2	0.061	0.33	1.52	5.69	0.56	151.54
		3	0.028	0.31	1.59	4.50	0.52	88.40
		4	0.039	0.49	1.03	4.22	0.37	85.74
		5	0.062	0.38	1.33	4.86	0.35	141.07
		6	0.049	0.32	1.55	4.90	0.51	139.16
		7	0.071	0.53	0.94	5.36	0.35	113.91
		8	0.049	0.30	1.66	5.57	0.52	125.85
		9	0.086	0.51	0.98	2.92	0.53	240.80
		10	0.096	0.42	1.06	3.84	0.44	247.54
		11	0.022	0.54	0.92	3.61	0.38	47.64
	2022	1	0.060	0.36	1.68	4.91	0.65	170.10
		2	0.060	0.35	1.70	5.73	0.59	166.68
		3	0.029	0.12	0.03	0.43	0.56	99.07
		4	0.039	0.52	1.16	4.29	0.40	94.48
		5	0.065	0.41	1.48	4.98	0.38	159.77
		6	0.051	0.35	1.73	4.98	0.55	156.95
		7	0.070	0.56	1.08	5.60	0.38	122.29
		8	0.052	0.33	1.83	5.58	0.55	144.68
		9	0.088	0.54	1.10	2.96	0.57	268.16
		10	0.090	0.44	1.17	3.86	0.47	254.68

		11	0.022	0.57	1.05	3.64	0.41	51.55
CON	2021	1	0.017	0.38	2.87	5.67	0.70	77.43
		2	0.049	0.37	3.00	8.35	0.66	168.70
		3	0.033	0.34	3.20	9.09	0.72	105.37
		4	0.004	0.50	2.20	7.92	0.65	9.88
		5	0.078	0.49	2.24	9.83	0.45	160.24
		6	0.039	0.33	3.20	8.33	0.61	132.99
	2022	1	0.017	0.46	4.12	6.01	0.91	102.33
		2	0.039	0.42	4.49	8.57	0.84	191.99
		3	0.032	0.41	4.60	9.78	0.87	137.18
		4	0.004	0.55	3.45	10.29	0.78	11.26
		5	0.086	0.62	3.05	9.96	0.53	233.69
		6	0.043	0.41	4.21	8.34	0.73	193.84

[a] Cross-sections numbered from downstream to upstream according to field surveys.
[b] Energy grade slope.

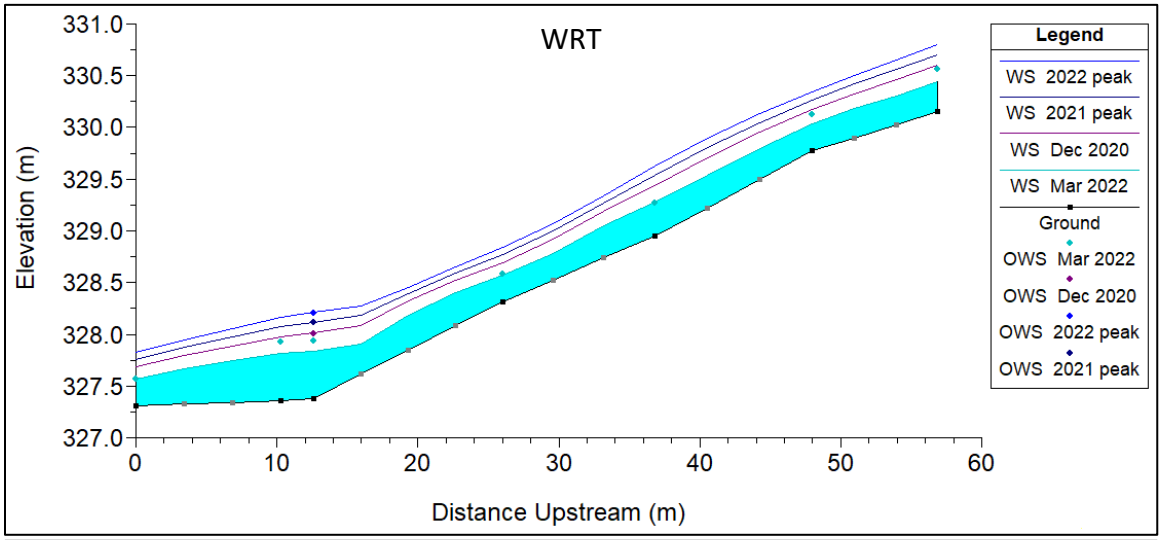

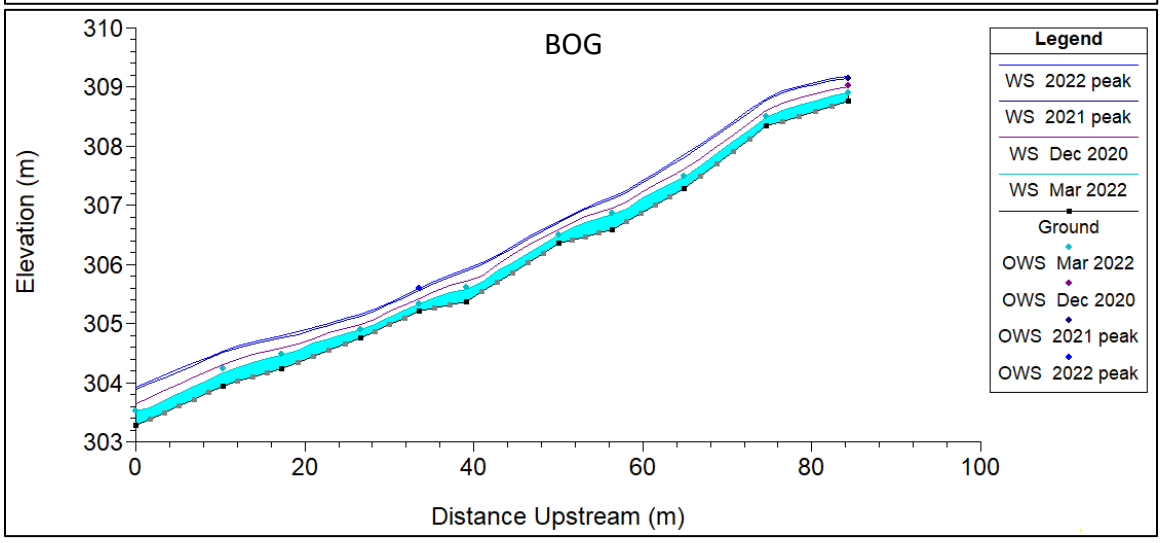

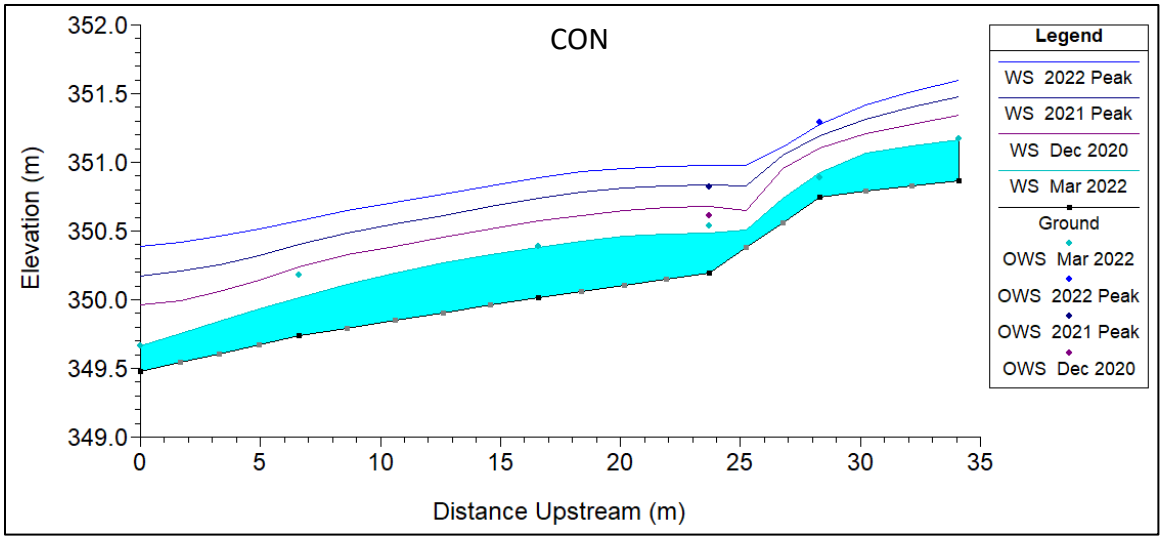

Figure A6. Water surface (WS) profiles from HEC-RAS modeling. When available, observed water surface (OWS) is indicated. Interpolated cross-sections displayed as gray dots. Axes scaled to data.

Precipitation

Table A3. Characteristics of precipitation data sources used in this study.

Data Source	Latitude	Longitude	Elevation (m)	Temporal Resolution	Distance to Study Sites	Available Dates
Archie1 tipping bucket gage	43.299731	-122.801334	619	1-min	in WRT basin	Nov. 2020 – Sep. 2021
Holiday4 tipping bucket gage	44.139128	-122.334849	405	1-min	3 km from CON	Nov. 2020 – Sep. 2021
USGS Blue River Dam Met Station near Blue River, OR, #441016122194300	44.171100	-122.328661	418	15-min	3 km from CON	Jan. 2021 – current
USGS Cougar Dam Met Station near Rainbow, OR, #440752122143200	44.131222	-122.242083	383	15-min	10 km from CON	July 2019 – current
PRISM Climate Group	–	–	–	1-day	spatially explicit	1981 – current

Hydrologic Response

Table A4. Summary of field measurements of discharge in burned sites using SonTek FlowTracker ADV.

Site	Dec-20		Jun-21		Mar-22	
	Q (m^3/s)	Uncertainty (%)	Q (m^3/s)	Uncertainty (%)	Q (m^3/s)	Uncertainty (%)
WRT	0.572	14.8	0.0671	12.2	0.2000	4.7
BOG	0.171	18.8	0.0134	40.8	0.0474	12.5
SWP[a]	0.088	10.1	–	–	0.0130	16.1
CON	0.487	7.6	0.0511	21.8	0.1014	11.1

[a] No measurement taken in Jun-21 due to low flows.

Table A5. Values used in back-calculations of Manning's *n* from topographic surveys and discharge measurements.

Site	Date[a]	Slope Method	*Q* (m^3/s)	*A* (m^2)	*P* (m)	*R* (m)	*S*	*n*
WRT	Dec-20	bed slope	0.572	1.841	5.533	0.333	0.029	0.262
WRT	Mar-22	WS slope	0.200	1.063	3.438	0.309	0.007	0.209
BOG	Dec-20	WS slope	0.171	0.311	2.638	0.118	0.049	0.096
BOG	Mar-22	WS slope	0.047	0.248	1.858	0.133	0.046	0.293
CON	Dec-20	bed slope	0.487	0.789	3.990	0.198	0.037	0.106
CON	Mar-22	WS slope	0.101	0.346	2.720	0.127	0.075	0.236

[a] I did not use discharge measurements from Jun-21 to estimate *n* because of low-flow conditions.

Table A6. Values used in peak discharge calculations determined from stage measurements and topographic surveys.

Site	Water Year	Slope Method	*n* Method	*A* (m^2)	*R* (m)	*S*	*n*	*Q* (m^3/s)
WRT	2021	Dec bed slope	Dec bed slope	4.11	0.28	0.029	0.262	1.138
WRT	2021	Mar WS	Mar WS	4.11	0.28	0.007	0.209	0.724
WRT	2022	Dec bed slope	Dec bed slope	5.39	0.32	0.029	0.262	1.632
WRT	2022	Mar WS	Mar WS	5.39	0.32	0.007	0.209	1.038
BOG	2021	Dec WS	Dec WS	0.92	0.22	0.049	0.096	0.767
BOG	2021	Dec WS	Mar WS	0.92	0.22	0.049	0.293	0.252
BOG	2022	Mar bed slope	Dec WS	1.50	0.25	0.051	0.096	1.390
BOG	2022	Mar bed slope	Mar WS	1.50	0.25	0.051	0.293	0.457
CON	2021	Mar WS	Dec bed slope	2.03	0.23	0.070	0.106	1.904
CON	2021	Mar WS	Mar WS	2.03	0.23	0.070	0.236	0.854
CON	2022	Mar WS	Dec bed slope	3.19	0.29	0.041	0.106	2.675
CON	2022	Mar WS	Mar WS	3.19	0.29	0.041	0.236	1.200

Table A7. Peak discharges (Q) and recurrence intervals (RI) for unregulated USGS gaged sites within 25 km of my study sites in the Archie Creek Fire.

USGS Gage Site	Boulder Cr. near Toketee Falls, OR, #14316495	Little R. at Peel, OR, #14318000	Steamboat Cr. Near Glide, OR, #14316700
Drainage Area (ha)	7.87E+03	4.58E+04	5.88E+04
% Catchment Burned	0	10	0
Gage Elevation (m)	500	255	343
Max Basin Elevation (m)	1859	1614	1822
2021 Peak Q Date	1/13/21	2/19/21	12/20/20
2021 Peak Q (m^3/s)	31.1	78.0	217
2021 Peak Unit Area $Q*10^8$ [$(m^3/s)/m^2$]	39.6	17.0	36.9
2021 Peak Q RI (yrs)	1.4	1.1	1.1
2022 Peak Q Date	1/7/22	1/6/22	1/7/22
2022 Peak Q (m^3/s)	32.3	109	204
2022 Peak Unit Area $Q*10^8$ [$(m^3/s)/m^2$]	41.0	23.8	34.7
2022 Peak Q RI (yrs)	1.5	1.2	1.1

Table A8. Peak discharges (Q) and recurrence intervals (RI) for unregulated gaged sites within 25 km of my study sites near the Holiday Farm Fire. WS1 and WS9 have unburned controls WS3 and WS10, respectively.

Gage Site	WS9	WS10[a]	WS2	WS1	WS3	Lookout Cr. near Blue R., OR, #14161500
Agency	HJA	HJA	HJA	HJA	HJA	USGS
Drainage Area (ha)	8.5	1.02E+01	6.00E+01	9.60E+01	1.01E+02	6.24E+03
% Catchment Burned	100	0	22	54	0	2
Gage Elevation (m)	426	461	545	439	476	435
Max Basin Elevation (m)	731	679	1079	1027	1080	1622
2021 Peak Q Date	9/19/21	12/20/20	12/20/20	12/20/20	12/20/20	12/20/20
2021 Peak Q (m^3/s)	0.07	0.08	0.36	0.71	0.55	42.2
2021 Peak Unit Area $Q*10^8$ [$(m^3/s)/m^2$]	81.7	81.6	60.7	73.5	54.7	67.6
2021 Peak Q RI (yrs)	2.2	1.5	1.7	1.3	1.4	1.7
2022 Peak Q Date	11/11/21	–	1/6/22	1/6/22	1/6/22	1/6/22
2022 Peak Q (m^3/s)	0.05	–	0.34	0.64	0.50	23.4
2022 Peak Unit Area $Q*10^8$ [$(m^3/s)/m^2$]	64.7	–	56.1	67.1	49.9	37.6

2022 Peak Q RI (yrs)	1.4	–	1.4	1.3	1.2	1.1

[a] Flow data was incomplete in 2022.

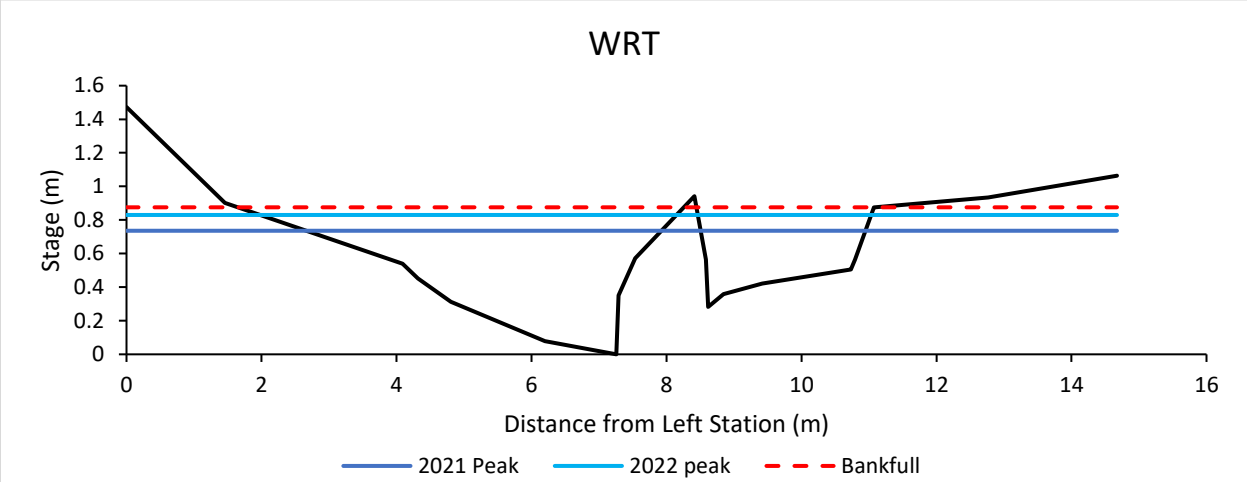

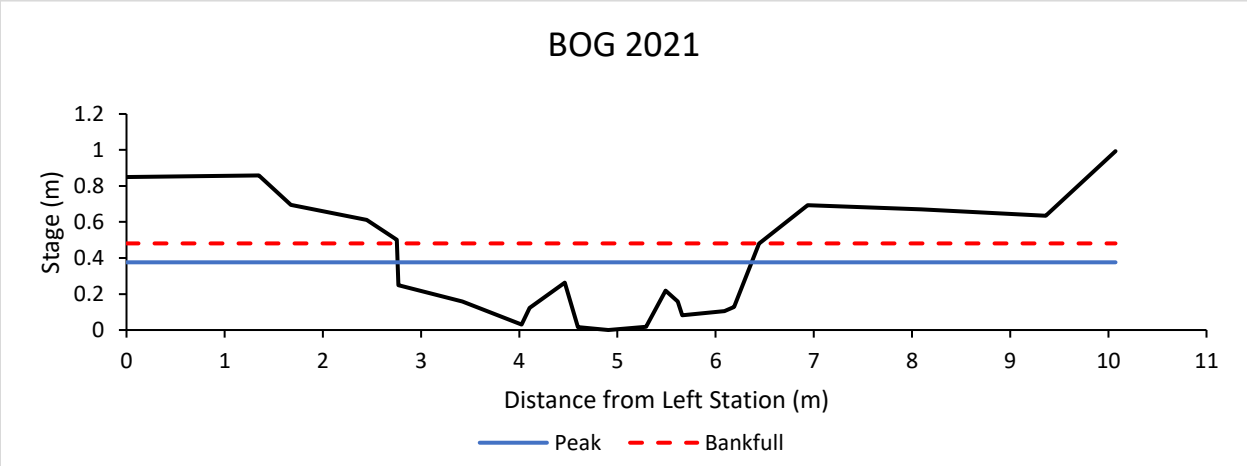

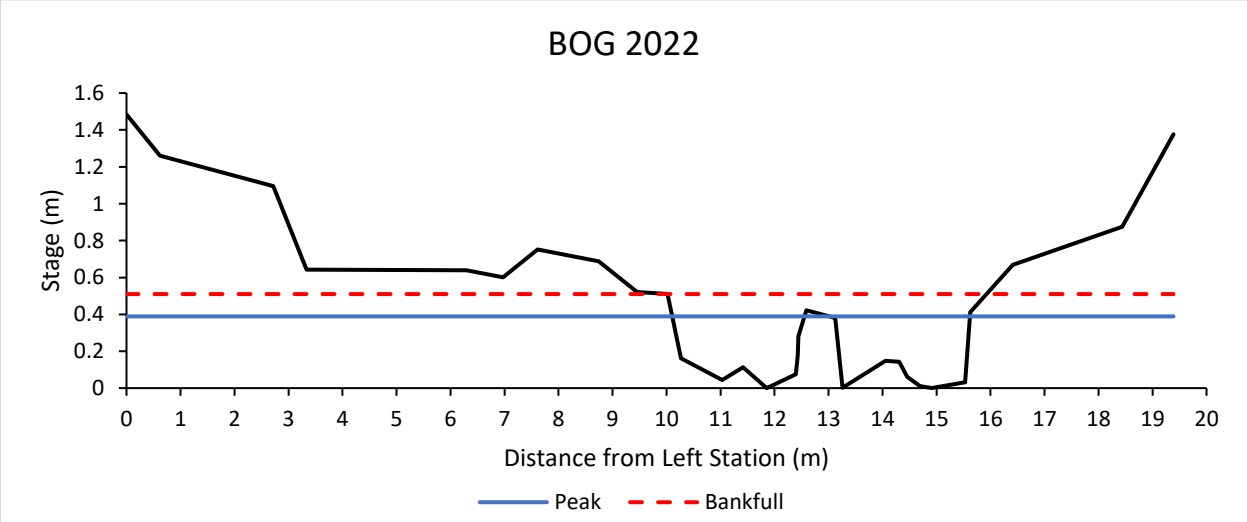

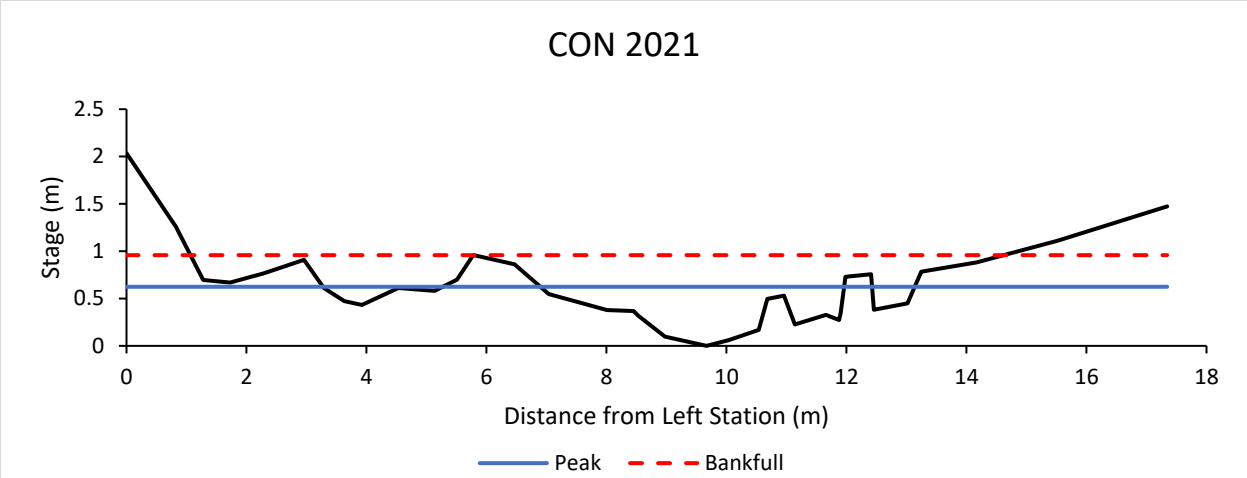

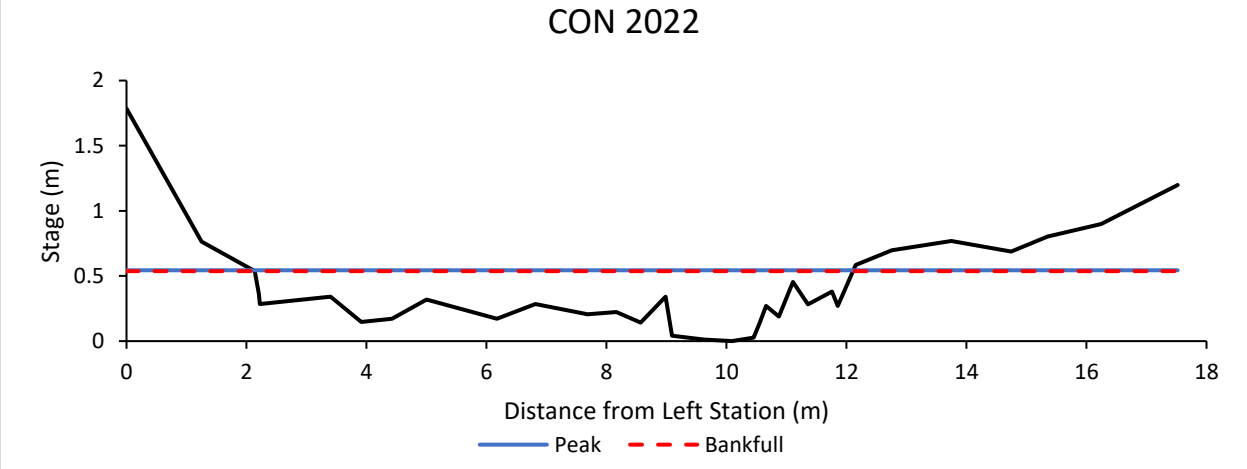

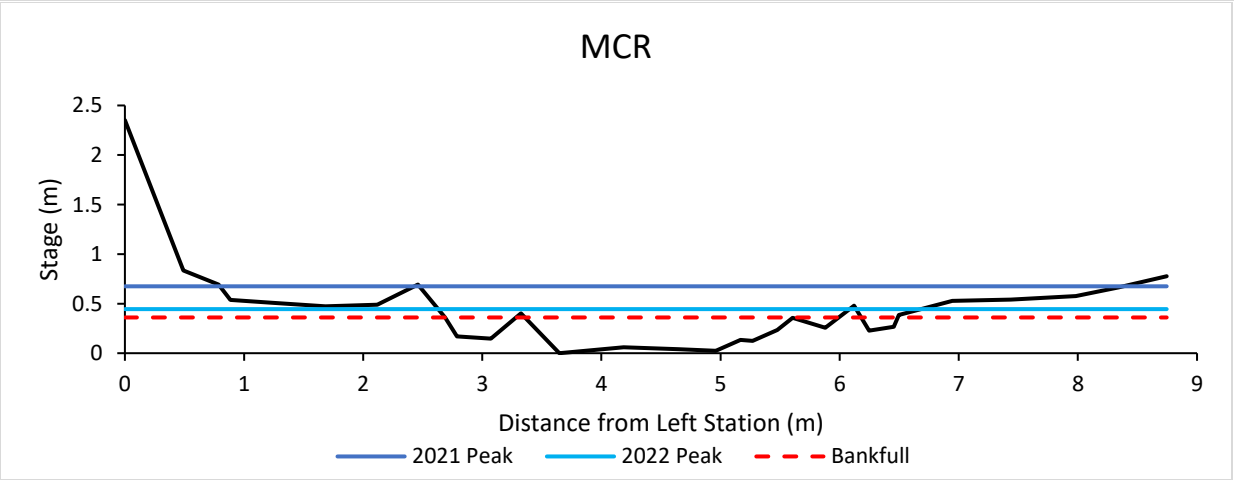

Figure A7. Peak flow stage at the pressure transducer cross-section in WYs 2021 and 2022. At all sites but WRT and MCR, the transducer was moved to a different location in Jun-21. Cross-section geometry for MCR is from August 2019.

Sediment inputs to study streams

Figure A8. Mar-22 orthophoto in WRT showing slide paths (black dashed polygons) and debris fans (red dashed ovals) from two landslides that occurred upstream of my study reach in January 2022. Blue arrow indicates flow direction.

Table A9. Characteristics of landslides in Wright Creek.

	Upstream Slide	Downstream Slide
Distance upstream of study reach (m)	700	600
Volume of erosion[a] (m^3)	900	1200
Sediment supplied to stream[a] (m^3)	750	300
Sediment delivery ratio[b] (%)	83	25
Contributing area[c] (km^2)	0.03	0.001
Slope of contributing area[c] (%)	52	–

[a] Estimated from UAV imagery-derived point cloud in Pix4D.

[b] SDR = sediment supplied to stream/volume of erosion.

[c] Calculated with ArcGIS spatial analyst. Contributing area of downstream slide was too small to calculate slope.

Fig. A9. The upstream landslide debris fan in WRT. The fan constricted the channel, forcing (A) a pool on the upstream side and (B) a drop on the downstream side.

Figure A10. Repeat photos in CON in (A) Jun-21 and (B) Mar-22 showing two slumps along the channel margin in (B). Blue arrow indicates flow direction.

Figure A11. Trail camera time-lapse photos looking upstream in WRT during (A) the 2021 peak flow on 13 January, (B) summer 2021 low flows, and (C) following the two landslides upstream of my study reach in January 2022.

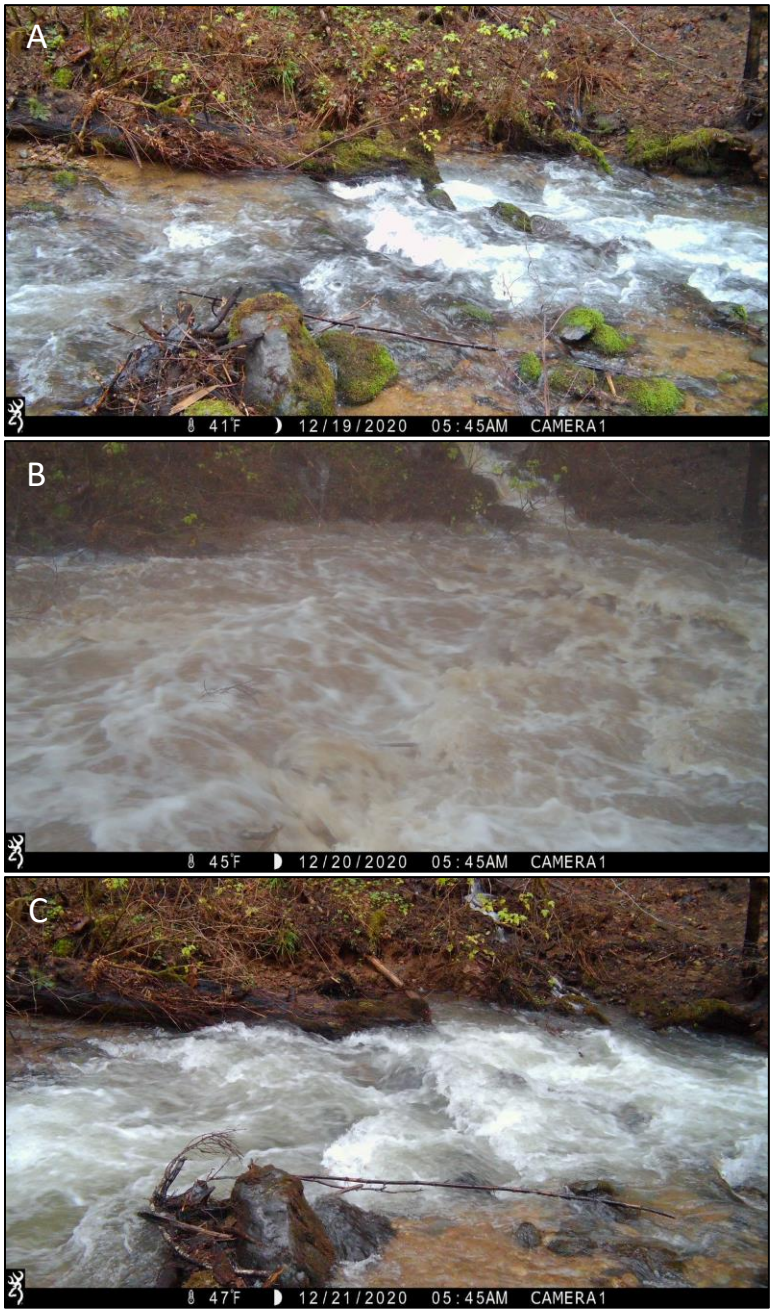

Figure A12. Trail camera time-lapse photos in CON (A) the day before, (B) the day of, and (C) the day after the peak flow on 20 December 2020. Note elevated suspended sediment in (B) and bank erosion between (A) and (C).

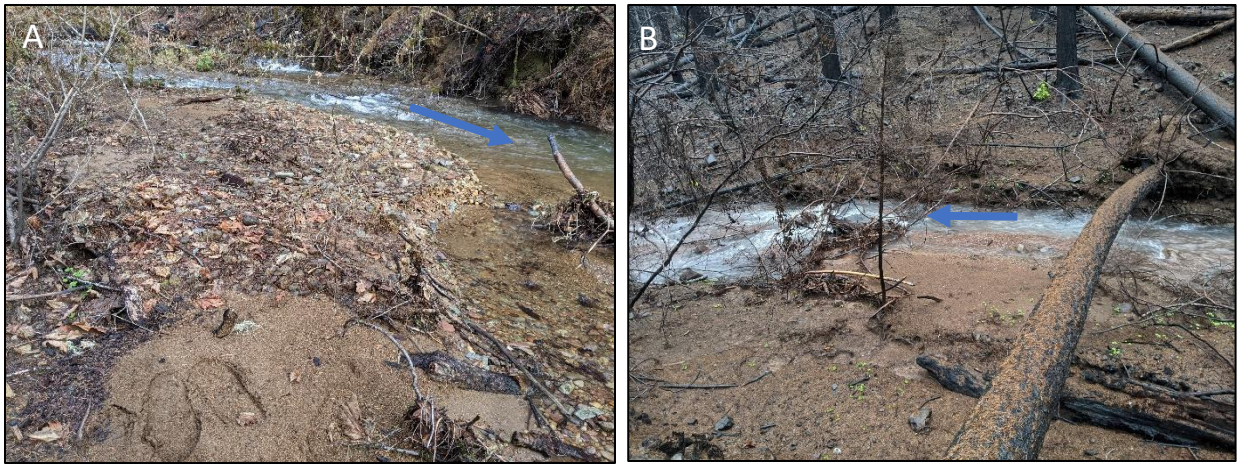

Figure A13. Overbank fine sediment deposition in (A) CON and (B) BOG in Dec-20. Blue arrow indicates flow direction.


Figure A14. View just above the upstream end of my study reach in BOG in Mar-22 showing a rill (dashed line) and associated sediment fan of fine to cobble-sized clasts (dashed oval). The rill was present in Dec-20 but it is unknown if it formed after the fires. 2 m survey pole on right side for scale. Blue arrow indicates flow direction.

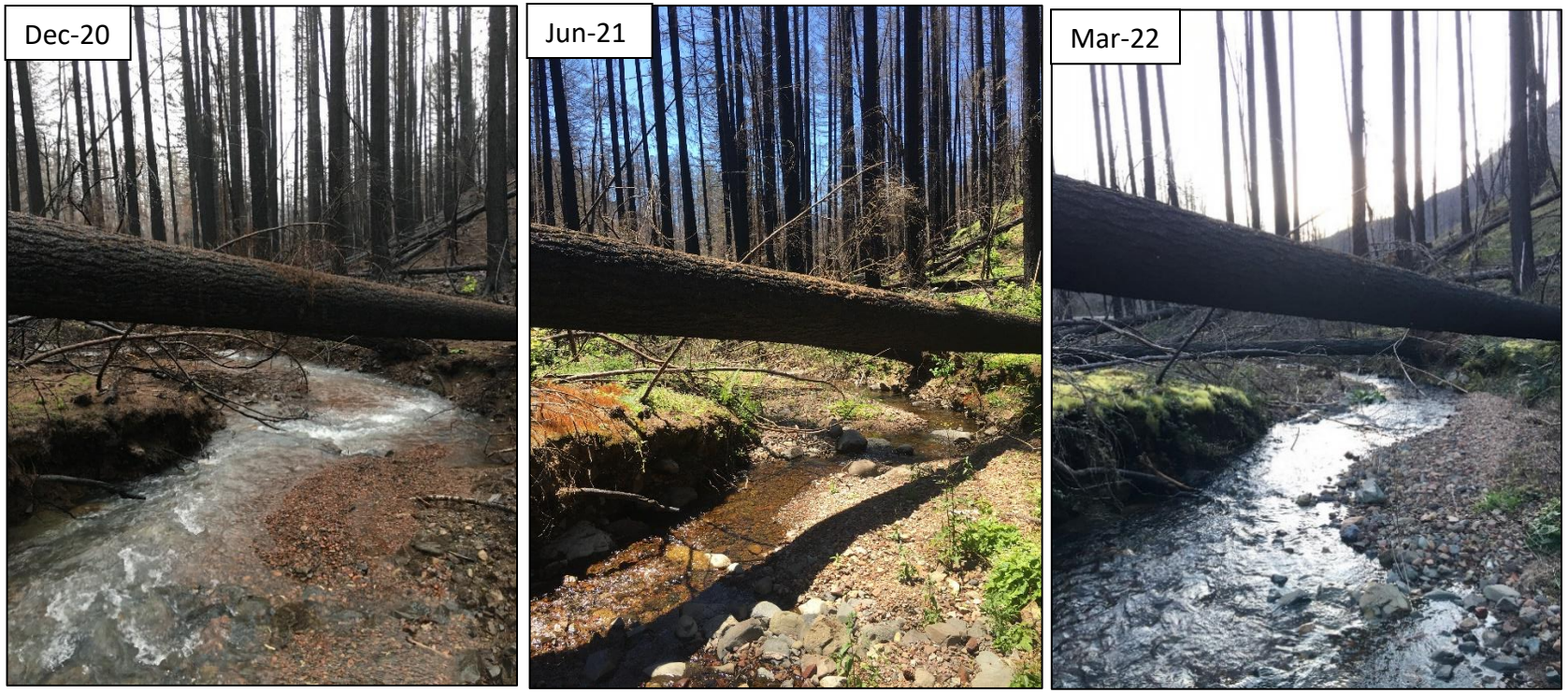

Fig. A15. Repeat photos in BOG showing a cutbank and stable marginal channel bar. The cutbank did not erode substantially during the study period.

Figure A16. Examples of recent bank collapse in SWP from (A) Dec-20 and (B) Mar-22. Blue arrows indicate flow direction.

Figure A17. Repeat photos looking downstream in SWP showing degradation of a large root wad and wood jam formation.

Geomorphic Response

Figure A18. Repeat photos looking upstream in BOG showing wood-forced gravel aggradation in (A) Jun-21 and subsequent erosion by (B) Mar-22 . There was >0.6 m of channel incision on the upstream end of the log in the photo. Hat on log in left photo for scale.

Figure A19. Repeat photos looking downstream in CON showing fine to cobble-sized sediment aggradation upstream of a channel-spanning large wood jam.

Table A10. Values used in calculations of flow competence and sediment mobility in study reaches.

Site	XS[a]	Water Year	S[b]	D_{50}[c] (m)	ρ_s (kg/m^3)	ρ (kg/m^3)	g (m/s^2)	R (m)	τ^*_c	τ_c (N/m^2)	τ_0[d] (N/m^2)	τ_0 / τ_c	Max mob. D[e] (m)
WRT	1	2021	0.037	0.054	2650	1000	9.81		0.061	53.0	83.6	1.6	0.085
WRT	2	2021	0.030	0.054	2650	1000	9.81		0.057	50.1	113.3	2.3	0.122
WRT	3	2021	0.011	0.054	2650	1000	9.81		0.044	38.4	34.8	0.9	0.049
WRT	4	2021	0.053	0.054	2650	1000	9.81		0.067	58.5	137.7	2.4	0.127
WRT	5	2021	0.073	0.054	2650	1000	9.81		0.073	63.8	225.5	3.5	0.191
WRT	7	2021	0.056	0.054	2650	1000	9.81		0.068	59.3	170.3	2.9	0.155
WRT	8	2021	0.049	0.054	2650	1000	9.81		0.065	57.1	168.9	3.0	0.160
WRT	1	2022	0.037	0.054	2650	1000	9.81		0.061	53.0	99.5	1.9	0.101
WRT	2	2022	0.033	0.054	2650	1000	9.81		0.059	51.4	143.9	2.8	0.151
WRT	3	2022	0.012	0.054	2650	1000	9.81		0.045	39.2	42.6	1.1	0.059
WRT	4	2022	0.055	0.054	2650	1000	9.81		0.068	59.2	165.4	2.8	0.151
WRT	5	2022	0.082	0.054	2650	1000	9.81		0.075	65.8	273.0	4.1	0.224

WRT	7	2022	0.056	0.054	2650	1000	9.81		0.068	59.4	207.8	3.5	0.189
WRT	8	2022	0.050	0.054	2650	1000	9.81		0.066	57.5	207.1	3.6	0.195
BOG	1	2021	0.060	0.023	2650	1000	9.81		0.069	25.8	155.4	6.0	0.139
BOG	2	2021	0.061	0.023	2650	1000	9.81		0.070	25.9	151.5	5.9	0.135
BOG	3	2021	0.028	0.023	2650	1000	9.81		0.056	20.9	88.4	4.2	0.097
BOG	4	2021	0.039	0.023	2650	1000	9.81		0.061	22.9	85.7	3.7	0.086
BOG	5	2021	0.062	0.023	2650	1000	9.81		0.070	26.0	141.1	5.4	0.125
BOG	6	2021	0.049	0.023	2650	1000	9.81		0.065	24.4	139.2	5.7	0.131
BOG	7	2021	0.071	0.023	2650	1000	9.81		0.072	27.0	113.9	4.2	0.097
BOG	8	2021	0.049	0.023	2650	1000	9.81		0.065	24.4	125.9	5.2	0.119
BOG	9	2021	0.086	0.023	2650	1000	9.81		0.076	28.4	240.8	8.5	0.195
BOG	10	2021	0.096	0.023	2650	1000	9.81		0.079	29.3	247.5	8.4	0.194
BOG	11	2021	0.022	0.023	2650	1000	9.81		0.053	19.5	47.6	2.4	0.056
BOG	1	2022	0.060	0.024	2650	1000	9.81		0.069	26.9	170.1	6.3	0.152
BOG	2	2022	0.060	0.024	2650	1000	9.81		0.069	26.9	166.7	6.2	0.149
BOG	3	2022	0.029	0.024	2650	1000	9.81		0.057	22.0	99.1	4.5	0.108
BOG	4	2022	0.039	0.024	2650	1000	9.81		0.061	23.9	94.5	4.0	0.095
BOG	5	2022	0.065	0.024	2650	1000	9.81		0.071	27.5	159.8	5.8	0.140
BOG	6	2022	0.051	0.024	2650	1000	9.81		0.066	25.7	157.0	6.1	0.147
BOG	7	2022	0.070	0.024	2650	1000	9.81		0.072	28.0	122.3	4.4	0.105
BOG	8	2022	0.052	0.024	2650	1000	9.81		0.067	25.8	144.7	5.6	0.134
BOG	9	2022	0.088	0.024	2650	1000	9.81		0.077	29.9	268.2	9.0	0.215
BOG	10	2022	0.090	0.024	2650	1000	9.81		0.077	30.1	254.7	8.5	0.203
BOG	11	2022	0.022	0.024	2650	1000	9.81		0.053	20.4	51.6	2.5	0.061
CON	1	2021	0.017	0.028	2650	1000	9.81		0.049	22.0	77.4	3.5	0.099
CON	2	2021	0.049	0.028	2650	1000	9.81		0.066	29.7	168.7	5.7	0.159
CON	3	2021	0.033	0.028	2650	1000	9.81		0.059	26.6	105.4	4.0	0.111
CON	4	2021	0.004	0.028	2650	1000	9.81		0.033	15.1	9.9	0.7	0.018
CON	5	2021	0.078	0.028	2650	1000	9.81		0.074	33.8	160.2	4.7	0.133
CON	6	2021	0.039	0.028	2650	1000	9.81		0.061	27.8	133.0	4.8	0.134

CON	1	2022	0.017	0.052	2650	1000	9.81		0.049	40.9	102.3	2.5	0.130
CON	2	2022	0.039	0.052	2650	1000	9.81		0.061	51.7	192.0	3.7	0.193
CON	3	2022	0.032	0.052	2650	1000	9.81		0.058	49.1	137.2	2.8	0.145
CON	4	2022	0.004	0.052	2650	1000	9.81		0.033	27.6	11.3	0.4	0.021
CON	5	2022	0.086	0.052	2650	1000	9.81		0.076	64.2	233.7	3.6	0.189
CON	6	2022	0.043	0.052	2650	1000	9.81		0.063	53.2	193.8	3.6	0.190
MCR		2021	0.015	0.078	2650	1000	9.81	0.28	0.047	59.7	41.2	0.7	0.054
MCR		2022	0.015	0.078	2650	1000	9.81	0.22	0.047	59.7	32.4	0.5	0.042

[a] Cross-sections from Mar-22 numbered from downstream to upstream according to field surveys. In MCR, used cross-section geometry at the pressure transducer from Aug-19.

[b] In burned study reaches, used energy grade slope from HEC-RAS. In MCR, used thalweg slope from Jun-21 topographic survey.

[c] In WRT and MCR, used D_{50} from Jun-21 pebble count for both 2021 and 2022 WYs.

[d] In burned study reaches, used values from HEC-RAS. In MCR, calculated values using equation, $\tau_0 = \rho g R S$.

[e] Maximum grain size mobilized.

Table A11. Bankfull depth and width values used in calculations of cross-section geometry change in burned study reaches.

	Dec-20			**Jun-21**			**Mar-22**		
Site	**XS #**[a]	**BF Depth (m)**	**BF Width (m)**	**XS #**[a]	**BF Depth (m)**	**BF Width (m)**	**XS #**[a]	**BF Depth (m)**	**BF Width (m)**
WRT	4	1.08	9.38	3	0.7	7.23	2	0.76	7.37
	5	0.8	8.18	4	0.55	5.61	3	0.88	9.44
	6	1.32	7.28	5	0.98	7.18	4	0.87	9.46
	7	0.908	6.54	6	0.912	5.36	5	0.82	8.04
	8	0.59	6.97	7	0.51	7.21	7	0.65	7.97
				8	0.41	8.53	8	0.63	6.71
BOG	1	0.93	8.16	1	0.75	8.72	1	0.72	5.15
	2	0.622	6.24	2	0.71	6.3	2	0.89	6.55
	3	0.48	5.92	3	0.4	6.09	3	0.41	4.38
	4	0.69	5.67	4	0.5	4.95	4	0.508	4.53
	5	0.33	4.92	5	0.52	4.72	5	0.51	5.91

	6	0.54	5.42	6	0.7	5.62	6	0.616	5.14
	7	0.56	5.21						
SWP	1	0.575	1.72	1	0.54	1.52	1	0.66	2.95
	2	0.36	2.7	2	0.6	2.29	2	0.606	2.07
	3	0.56	3.32	3	0.61	3.42	3	0.82	3.06
	4	0.49	2.24	4	0.35	2.43	4	0.41	1.97
	5	0.44	2.04	5	0.46	2.34	5	0.77	2.39
							6	0.573	1.96
CON	1	0.32	7.18	1	0.596	6.78	1	1.15	6.42
	2	0.36	7.57	2	0.444	8.5	2	0.725	8.52
	3	0.82	11.44	3	0.41	8.65	3	0.73	9.62
	4	0.52	10.77	4	0.597	10.57	4	0.96	13.55
	5	0.58	7.89	5	0.44	10.16	5	0.54	9.97
				6	0.92	9.42	6	0.45	7.27

[a] Cross-sections used in channel change calculations are independent across surveys and cover the same section of the reach. Cross-sections are numbered downstream to upstream according to field surveys.

Table A12. Wright Creek pebble count data from field surveys. Pebble counts were conducted in the same section of the reach across surveys by zigzagging along the channel and selecting particles at random. Boulders were excluded from the count.

Count	Jun-21		Mar-22		Mar-22 Above Jam		Mar-22 Below Jam	
	Diam. (mm)	% Finer	Diam. (mm)	% Finer	Diam. (mm)	% Finer	Diam. (mm)	% Finer
1	<2	0	<2	0	<2	0	<2	0
2	<2	0	<2	0	<2	0	<2	0
3	<2	0	<2	0	<2	0	<2	0
4	<2	0	<2	0	<2	0	<2	0
5	2	4	<2	0	<2	0	<2	0
6	3	5	<2	0	<2	0	<2	0
7	3	5	<2	0	5	21	<2	0
8	3	5	<2	0	6	25	<2	0
9	5	8	<2	0	6	25	<2	0

10	5	8	<2	0	7	32	<2	0
11	6	10	<2	0	7	32	<2	0
12	7	11	<2	0	10	39	6	15
13	9	12	<2	0	14	43	10	17
14	10	13	<2	0	16	46	11	18
15	10	13	<2	0	20	50	15	19
16	12	<2	<2	0	27	54	19	21
17	12	15	<2	0	38	57	23	22
18	12	15	6	17	47	61	23	22
19	14	18	7	18	49	64	24	25
20	15	19	10	19	50	68	26	26
21	15	19	11	20	59	71	26	26
22	16	21	21	21	59	71	28	29
23	17	22	22	22	78	79	29	31
24	17	22	26	23	115	82	35	32
25	19	24	28	24	126	86	37	33
26	20	25	32	25	127	89	41	35
27	21	26	34	26	135	93	43	36
28	22	27	35	27	202	96	49	38
29	27	28	35	27			53	39
30	28	29	39	29			54	40
31	28	29	40	30			56	42
32	30	31	42	31			57	43
33	30	31	42	31			59	44
34	30	31	44	33			64	46
35	31	34	45	34			66	47
36	31	34	45	34			71	49
37	34	36	49	36			73	50
38	35	37	50	37			77	51
39	38	38	56	38			79	53

40	39	39	61	39			79	53
41	39	39	61	39			79	53
42	39	39	63	41			85	57
43	40	42	71	42			85	57
44	41	43	71	42			96	60
45	43	44	72	44			99	61
46	45	45	75	45			100	63
47	45	45	76	46			100	63
48	46	47	79	47			110	65
49	47	48	80	48			111	67
50	49	49	80	48			112	68
51	54	50	81	50			114	69
52	55	51	82	50			118	71
53	55	51	84	51			118	71
54	56	53	85	52			119	74
55	57	54	85	52			122	75
56	57	54	87	54			126	76
57	59	56	95	55			130	78
58	60	57	95	55			134	79
59	60	58	100	57			134	79
60	60	58	101	58			139	82
61	61	60	105	59			148	83
62	62	61	108	60			149	85
63	63	62	109	61			157	86
64	64	63	109	61			176	88
65	69	64	110	63			176	88
66	70	65	110	63			182	90
67	72	66	112	65			196	92
68	73	67	112	65			199	93
69	73	67	113	67			214	94

70	75	69	114	68			234	96
71	75	69	117	69			235	97
72	76	71	121	70			243	99
73	82	72	122	71				
74	84	73	126	72				
75	85	74	127	73				
76	89	75	129	74				
77	89	75	130	75				
78	90	77	134	76				
79	95	78	139	77				
80	97	79	146	78				
81	105	80	148	79				
82	114	81	148	79				
83	119	82	150	81				
84	125	83	150	81				
85	125	83	150	81				
86	126	85	150	81				
87	130	86	152	85				
88	135	87	154	86				
89	137	88	160	87				
90	144	89	164	88				
91	148	90	165	89				
92	155	91	168	90				
93	157	92	178	91				
94	170	93	179	92				
95	176	94	180	93				
96	176	94	195	94				
97	190	96	198	95				
98	190	96	200	96				
99	200	98	208	97				

100	206	99	238	98				
101			240	99				

Table A13. Bogus Creek pebble count data from field surveys. Pebble counts were conducted in the same section of the reach across surveys by zigzagging along the channel and selecting particles at random. Boulders were excluded from the count.

Count	Dec-20		Jun-21		Mar-22	
	Diam. (mm)	% Finer	Diam. (mm)	% Finer	Diam. (mm)	% Finer
1	<2	0	<2	0	<2	0
2	3	1	<2	0	<2	1
3	5	2	<2	0	3	2
4	5	2	<2	0	4	3
5	6	4	4	4	4	3
6	6	4	4	4	4	3
7	7	6	6	6	4	3
8	7	6	6	6	5	7
9	7	6	7	8	5	7
10	7	6	7	8	6	9
11	8	10	7	8	6	9
12	9	11	7	8	7	11
13	9	11	8	12	8	12
14	9	11	8	12	9	13
15	9	11	8	12	9	13
16	10	15	8	12	9	13
17	10	15	8	12	10	16
18	10	15	9	17	10	16
19	11	18	9	17	10	16
20	11	18	10	19	11	19
21	11	18	11	20	11	19
22	12	21	11	20	11	19
23	12	21	11	20	11	19

24	13	23	11	20	11	19
25	14	24	11	20	11	19
26	14	24	12	25	13	25
27	14	24	12	25	13	25
28	14	24	13	27	13	25
29	14	24	13	27	14	28
30	14	24	13	27	16	29
31	15	30	14	30	17	30
32	16	31	16	31	18	31
33	16	31	17	32	19	32
34	16	31	18	33	19	32
35	17	34	18	33	20	34
36	17	34	18	33	21	35
37	17	34	18	33	21	35
38	18	37	18	33	21	35
39	18	37	19	38	21	35
40	18	37	20	39	22	39
41	18	37	20	39	23	40
42	18	37	21	41	26	41
43	19	42	21	41	26	41
44	19	42	21	41	26	41
45	20	44	22	44	26	41
46	20	44	24	45	30	45
47	20	44	24	45	31	46
48	20	44	24	45	31	46
49	22	48	24	45	32	48
50	22	48	24	45	35	49
51	23	50	24	45	36	50
52	23	50	25	50	39	51
53	23	50	26	51	39	51

54	23	50	27	52	40	53
55	23	50	27	52	41	54
56	25	55	27	52	41	54
57	26	56	27	52	42	56
58	26	56	28	56	44	57
59	27	58	29	57	46	58
60	27	58	29	57	46	58
61	28	60	29	57	48	60
62	28	60	30	60	48	60
63	30	62	32	61	51	62
64	30	62	34	62	54	63
65	30	62	34	62	54	63
66	30	62	36	64	55	65
67	32	66	39	65	57	66
68	32	66	40	66	58	67
69	32	66	41	67	59	68
70	33	69	44	68	59	68
71	34	70	45	69	60	70
72	34	70	46	70	63	71
73	36	72	47	71	65	72
74	37	73	48	72	66	73
75	38	74	48	72	68	74
76	38	74	49	74	69	75
77	38	74	50	75	71	76
78	39	77	53	76	75	77
79	39	77	54	77	76	78
80	40	79	54	77	77	79
81	42	80	54	77	78	80
82	42	80	54	77	78	80
83	42	80	55	81	80	82

84	43	83	58	82	84	83
85	47	84	58	83	97	84
86	47	84	58	83	99	85
87	52	86	60	85	99	85
88	52	86	61	86	105	87
89	52	86	63	87	105	87
90	54	89	68	88	113	89
91	78	90	78	89	118	90
92	91	91	78	89	119	91
93	102	92	103	91	128	92
94	124	93	104	92	138	93
95	138	94	105	93	138	93
96	140	95	114	94	148	95
97	160	96	115	95	152	96
98	234	97	115	95	191	97
99	235	98	138	97	202	98
100	245	99	158	98	256	99
101			190	99		

Table A14. Swamp Creek pebble count data from field surveys. Pebble counts were conducted in the same section of the reach across surveys by zigzagging along the channel and selecting particles at random. Boulders were excluded from the count.

Count	Dec-20		Jun-21		Mar-22	
	Diam. (mm)	% Finer	Diam. (mm)	% Finer	Diam. (mm)	% Finer
1	<2	0	<2	0	<2	0
2	<2	0	<2	0	<2	0
3	<2	0	<2	0	<2	0
4	<2	0	<2	0	<2	0
5	<2	0	<2	0	<2	0
6	<2	0	<2	0	<2	0
7	<2	0	<2	0	<2	0

8	<2	0	<2	0	<2	0
9	<2	0	<2	0	<2	0
10	<2	0	<2	0	<2	0
11	<2	0	<2	0	<2	0
12	<2	0	<2	0	<2	0
13	<2	0	<2	0	<2	0
14	<2	0	<2	0	<2	0
15	<2	0	<2	0	<2	0
16	<2	0	<2	0	<2	0
17	<2	0	<2	0	<2	0
18	<2	0	<2	0	<2	0
19	<2	0	<2	0	<2	0
20	<2	0	<2	0	<2	0
21	<2	0	<2	0	<2	0
22	<2	0	<2	0	<2	0
23	<2	0	<2	0	<2	0
24	<2	0	<2	0	<2	0
25	<2	0	<2	0	<2	0
26	<2	0	<2	0	<2	0
27	<2	0	<2	0	<2	0
28	<2	0	<2	0	<2	0
29	<2	0	<2	0	<2	0
30	<2	0	3	29	<2	0
31	<2	0	3	29	<2	0
32	<2	0	4	31	<2	0
33	<2	0	4	31	<2	0
34	<2	0	4	31	<2	0
35	<2	0	4	31	<2	0
36	<2	0	5	35	<2	0
37	<2	0	5	35	<2	0

38	<2	0	5	35	5	37
39	<2	0	5	35	6	38
40	<2	0	6	39	6	38
41	<2	0	6	39	7	40
42	<2	0	7	41	7	40
43	<2	0	7	41	8	42
44	<2	0	7	41	8	42
45	<2	0	7	41	9	44
46	3	49	8	45	9	44
47	3	49	9	46	10	46
48	3	49	9	46	11	47
49	3	49	9	46	11	47
50	3	49	9	46	11	47
51	3	49	9	46	12	50
52	4	56	9	46	12	50
53	4	56	9	46	13	52
54	4	56	10	53	14	53
55	4	56	10	53	14	53
56	5	60	10	53	14	53
57	5	60	10	53	15	56
58	5	60	11	57	15	56
59	6	60	11	57	15	56
60	6	60	11	57	15	56
61	7	66	11	57	17	60
62	7	66	12	61	18	61
63	8	68	12	61	21	62
64	8	68	13	63	23	63
65	10	70	15	64	24	64
66	10	70	15	64	27	65
67	10	70	15	64	29	66

68	10	70	16	67	34	67
69	11	75	17	68	35	68
70	12	76	20	69	36	69
71	12	76	21	70	51	70
72	15	78	22	71	58	71
73	16	79	22	71	60	72
74	18	80	24	73	60	72
75	18	80	25	74	61	74
76	20	82	26	75	61	74
77	25	84	26	75	71	76
78	28	85	27	77	72	77
79	31	86	34	78	76	78
80	48	87	36	79	79	79
81	57	88	39	80	84	80
82	88	89	40	81	85	81
83	100	90	43	82	86	82
84	105	91	46	83	86	82
85	110	92	48	84	93	84
86	112	93	53	85	94	85
87	118	95	58	86	96	86
88	142	96	60	87	111	87
89	205	97	62	88	112	88
90	210	98	67	89	114	89
91	225	99	71	90	116	90
92			73	91	119	91
93			92	92	120	92
94			95	93	127	93
95			97	94	137	94
96			100	95	138	95
97			105	96	153	96

98			105	96	168	97
99			111	98	213	98
100			132	99	219	99

Table A15. Cone Creek pebble count data from field surveys. Pebble counts were conducted in the same section of the reach across surveys by zigzagging along the channel and selecting particles at random. Boulders were excluded from the count.

Count	Dec-20		Jun-21		Mar-22	
	Diam. (mm)	% Finer	Diam. (mm)	% Finer	Diam. (mm)	% Finer
1	1	0	1	0	1	0
2	1	0	8	1	1	0
3	1	0	9	2	1	0
4	1	0	10	3	3	3
5	1	0	10	3	6	4
6	1	0	11	5	7	5
7	1	0	11	5	7	5
8	1	0	11	5	11	7
9	1	0	11	5	11	7
10	1	0	11	5	11	7
11	1	0	12	10	11	7
12	2	13	12	10	12	11
13	2	13	12	10	12	11
14	3	15	13	13	13	13
15	3	15	15	14	15	14
16	4	17	15	14	15	14
17	4	17	16	16	16	16
18	5	20	17	17	17	17
19	5	20	19	18	18	18
20	5	20	20	19	19	19
21	5	20	20	19	20	20
22	6	24	21	21	20	20

23	8	25	21	21	21	22
24	8	25	22	23	21	22
25	8	25	25	24	24	24
26	8	25	26	25	24	24
27	9	30	26	25	26	26
28	9	30	27	27	27	27
29	9	30	27	27	27	27
30	11	33	28	29	27	27
31	11	33	29	30	28	30
32	14	36	29	30	29	31
33	17	37	31	32	29	31
34	19	38	31	32	29	31
35	19	38	32	34	29	31
36	19	38	32	34	30	35
37	20	41	32	34	30	35
38	20	41	33	37	30	35
39	20	41	33	37	32	38
40	20	41	33	37	33	39
41	22	46	34	40	33	39
42	25	47	35	41	35	41
43	26	48	36	42	35	41
44	28	49	40	43	36	43
45	28	49	42	44	36	43
46	28	49	43	45	37	45
47	28	49	45	46	39	46
48	29	54	49	47	40	47
49	30	55	50	48	43	48
50	30	55	51	49	44	49
51	31	57	52	51	46	50
52	32	59	55	52	47	50

53	32	59	55	52	50	51
54	33	61	55	52	50	51
55	35	62	55	52	52	53
56	36	63	57	56	53	54
57	40	64	58	57	55	55
58	42	66	58	57	56	56
59	42	66	58	57	56	56
60	46	68	59	60	56	56
61	49	69	61	61	58	59
62	54	70	61	61	59	60
63	55	71	62	63	59	60
64	55	71	64	64	59	60
65	58	74	66	65	61	63
66	59	75	68	66	62	64
67	60	76	68	66	66	65
68	60	76	71	68	68	66
69	60	76	72	69	69	67
70	62	79	73	70	70	68
71	65	80	75	71	72	69
72	65	80	75	71	77	70
73	65	80	76	73	78	71
74	70	84	78	74	80	72
75	80	85	80	75	86	73
76	80	85	81	76	91	74
77	85	87	82	77	91	74
78	90	89	82	77	91	74
79	91	90	85	79	93	77
80	92	91	85	79	96	78
81	95	92	87	81	97	79
82	95	92	90	82	98	80

83	101	94	95	83	110	81
84	110	95	100	84	114	82
85	114	97	102	85	114	82
86	115	98	112	86	118	84
87	168	99	113	87	131	85
88			117	88	136	86
89			118	89	142	87
90			125	90	144	88
91			132	91	149	89
92			133	92	152	90
93			160	93	153	91
94			176	94	158	92
95			181	95	161	93
96			185	96	169	94
97			210	97	175	95
98			236	98	179	96
99			245	99	180	97
100					202	98
101					224	99

Table A16. McRae Creek cross-section pebble count data. Pebble counts were conducted at the same cross-section across surveys by selecting particles at random and measuring with a gravelometer. August 2019 count was conducted by NEON staff.

Aug-19			**Jun-21**		
Size Class (mm)	**Number**	**% Finer**	**Size Class (mm)**	**Number**	**% Finer**
2	1	0	2	1	0
5.6	0	0	2.8	1	2.5
8	1	2.5	5.6	1	5
11	2	5	8	3	7.5
16	2	10	11	2	15
22.6	4	15	16	2	20

32	3	25	22.6	5	25
45	3	32.5	32	2	37.5
64	5	40	45	4	42.5
90	4	52.5	56	1	52.5
128	5	62.5	64	5	55
180	3	75	90	2	67.5
256	2	82.5	120	1	72.5
>256	5	87.5	128	4	75
			172	4	85
			>172	2	95

Table A17. McRae Creek reach pebble count data from Jun-21 field survey. Pebble count was conducted by zigzagging along the channel and selecting particles at random. Boulders were excluded from the count.

Count	**Diam. (mm)**	**% Finer**
1	1	0
2	2	1
3	3	2
4	5	3
5	7	4
6	8	5
7	10	6
8	10	6
9	10	6
10	10	6
11	11	10
12	11	10
13	12	12
14	13	13
15	13	13
16	13	13

17	15	16
18	16	17
19	17	18
20	19	19
21	20	20
22	24	21
23	25	22
24	28	23
25	30	24
26	30	24
27	34	26
28	34	26
29	36	28
30	37	29
31	38	30
32	41	31
33	41	31
34	43	33
35	45	34
36	52	35
37	53	36
38	56	37
39	58	38
40	58	38
41	59	40
42	60	41
43	60	41
44	61	43
45	68	44
46	69	45

47	76	46
48	77	47
49	77	47
50	77	47
51	78	50
52	79	51
53	80	52
54	80	52
55	83	54
56	90	55
57	90	55
58	90	55
59	92	58
60	92	58
61	94	60
62	99	61
63	104	62
64	105	63
65	106	64
66	110	65
67	110	65
68	111	67
69	114	68
70	115	69
71	115	69
72	115	69
73	118	72
74	120	73
75	134	74
76	135	75

77	138	76
78	139	77
79	140	78
80	140	78
81	143	80
82	148	81
83	154	82
84	155	83
85	159	84
86	162	85
87	164	86
88	165	87
89	175	88
90	177	89
91	180	90
92	189	91
93	191	92
94	192	93
95	200	94
96	206	95
97	220	96
98	220	96
99	222	98
100	235	99

Instream Wood

Figure A20. Repeat photos in WRT showing post-fire treefall between (A) Jun-21 and (B) Mar-22.

Table A18. Large wood (LW) quantities in study reaches.

Site	LW pieces/100 m stream length
WRT	18.3
BOG	10.3
SWP	16.4
CON	14.0
MCR	9.4

Table A19. Large wood classifications in study reaches.

Site	Piece #	Class-ification	Rootwad	Features of Accumulation	Level of Decay	Burn Status	Stability	Source	Forcing Geomorphic Unit
WRT[a]	1	jam 1	yes	rootwad; channel spanning jam	bark	unburned	ramp	riparian	pool
	2	jam 1	no	channel spanning jam	bark	unburned	ramp	unknown	pool
	3	jam 1	no	channel spanning jam	bark	unburned	unattached	unknown	pool
	4	jam1	no	channel spanning jam	bark	unburned	pinned	unknown	pool
	5	jam1	no	channel spanning jam	bare	completely	pinned	unknown	pool
	6	jam 1	no	channel spanning jam	bare	unknown	pinned	unknown	pool
	7	single	no	none	bare	completely	ramp	riparian/hillslope	none
	8	single	no	none	bark	partial	unattached	unknown	none
	9	single	no	rootwad	bark	partial	collapsed bridge	hillslope	none
	10	single	no	boulder	bark	unknown	unattached	unknown	none
	11	single	no	small wood (<20 cm diameter) jam	bare	partial	unattached	unknown	none
	12	single	no	none	bare	completely	ramp	riparian/hillslope	none
	13	single	no	rootwad	bare	completely	ramp	riparian	none
BOG[a]	1	single	no	none	bark	completely	bridge	riparian	no
	2	single	no	marginal channel bar	bark	completely	unattached	unkown	marginal channel bar
	3	single	no	marginal channel bar; flush with DS LW	bark	partial	unattached	unknown	marginal channel bar
	4	single	no	none	bark	completely	ramp	riparian	no
	5	single	no	marginal channel bar; pinned	bark	partial	pinned	unknown	marginal channel bar
	6	single	yes	rootwad	bark	completely	bridge	bank undercutting	mid-channel bar
	7	single	yes	rootwad	bark	completely	ramp	bank undercutting	no
	8	single	no	mid-channel bar	bark	completely	ramp	riparian	mid-channel bar
	9	single	no	buried in bed	bare	completely	ramp; buried	riparian	mid-channel bar
	10	single	no	none	bark	completely	unattached	unknown	no
	11	single	no	none	bare	unknown	unattached	unknown	no

	12	single	no	none	bark	completely	bridge	riparian	no
SWP[a]	1	single	no	rootwad	bark	completely	bridge	riparian	none
	2	single	no	caught on step	bare	completely	unattached	unknown	none
	3	jam 1	no	channel spanning jam	bark	completely	pinned; ramp	riparian	none
	4	jam 1	no	rootwad; channel spanning jam	bark	partial	bridge	riparian	none
	5	jam 1	no	channel spanning jam	bark	partial	pinned; ramp	riparian	none
	6	jam 1	no	channel spanning jam	needles	partial	pinned; ramp	riparian	none
	7	jam 1	no	channel spanning jam	bark	partial	pinned; ramp	riparian	none
	8	jam 1	no	channel spanning jam	decayed	completely	pinned	unknown	none
	9	jam 1	no	channel spanning jam	decayed	completely	ramp	unknown	none
	10	jam 1	no	channel spanning jam	bark	partial	ramp	unknown	none
	11	single	no	none	bare	completely	unattached	unknown	none
	12	single	no	none	bare	completely	pinned; ramp	unknown	none
	13	single	no	none	rotten	completely	unattached	unknown	none
	14	single	no	none	bare	completely	unattached	unknown	none
	15	single	no	none	decayed	completely	unattached	unknown	none
	16	single	no	none	bare	completely	ramp	hillslope	none
	17	single	no	none	rotten	completely	unattached	hillslope	none
	18	single	no	none	rotten	completely	bridge	riparian/hillslope	none
	19	single	no	none	bare	completely	unattached	unknown	none
CON[a]	1	single	no	none	rotten	completely	ramp	hillslope	none
	2	single	no	none	decayed	completely	ramp	hillslope	none
	3	jam 1	no	channel spanning jam	bark	partial	ramp	hillslope	pool; bar
	4	jam 1	no	channel spanning jam	bare	unknown	unattached	unknown	none
	5	jam 1	no	channel spanning jam	bare	unknown	pinned	unknown	pool; bar
	6	single	no	boulder	decayed	completely	unattached	fluvial	none
	7	single	no	none	bare	completely	ramp	riparian	none
	8	single	no	boulder	bare	partial	unattached	unknown	none
	9	single	no	boulder	decayed	completely	unattached	unknown	none

	10	single	no	none	decayed	completely	collapsed bridge	riparian	none
	11	single	no	none	decayed	completely	bridge	riparian	none
	12	single	no	none	bare	completely	unattached	unknown	none
	13	single	no	bar	bare	completely	pinned	unknown	none
	14	single	no	none	rotten	completely	unattached	riparian/hillslope	none
	15	single	no	none	decayed	completely	unattached	riparian/hillslope	none
MCR[b]	1	single	no	log step; boulder	decayed	unburned	unattached	unknown	step
	2	single	no	none	bare	unburned	collapsed bridge	riparian/hillslope	bar
	3	single	no	marginal channel bar; flush with DS LW	decayed	unburned	unattached	unknown	none
	4	single	no	buried	bare	unburned	ramp; buried	riparian/hillslope	none
	5	single	no	log step	bare	unburned	pinned	riparian/hillslope	bar; step

[a] Large wood conditions in Mar-22.

[b] Large wood conditions in Jun-21.

Precipitation Thresholds for Debris Flows

To assess whether precipitation thresholds for debris flow initiation were exceeded during the study period, I examined published debris flow rainfall thresholds in western Oregon. Debris flow thresholds are typically developed using either statistical or empirical methods. USGS statistical models classified three of my burned sites as having high debris flow hazard in response to a 15-min, 24 mm hr^{-1} rain event (USGS, 2020). This rain intensity is at the low end of most western United States convective thunderstorms and at the upper end of intensities for the stratiform rainfall typical of western Oregon. Examining precipitation in study sites indicates this threshold was not exceeded during the study period (Table 2). Although statistical models of debris flow likelihood and magnitude are useful in identifying high-hazard areas, they are not meant to be used as a predictive tool (Staley et al., 2017).

Empirical approaches for developing rainfall intensity-duration thresholds rely on extensive historical data on rainfall and basin response (Staley et al., 2017). While these thresholds are well characterized across semiarid regions of the western United States (e.g., Staley et al., 2017; Raymond et al., 2020), there is a paucity of these data for western Oregon. Debris flows in western Oregon differ from those in semiarid regions in that they are typically initiated from saturation-induced shallow landslides. This requires that soils are thoroughly rewetted following the summer dry season, adding a substantial antecedent rainfall component to precipitation thresholds (Wiley, 2000). Wiley (2000) suggests as a preliminary, conservative threshold, that debris flows (here, inclusive of all "fast-moving landslides," not just true debris flows) in western Oregon will occur where ~20 cm of antecedent rain has fallen since the end of September and 24-hour rainfall exceeds 40% of mean December rainfall. This threshold does not consider wildfire, which increases debris flow likelihood (e.g., Shakesby and Doerr, 2006). Land development, including forest road construction, may also influence thresholds due to over-steepened slopes, artificial fill, and concentration of drainage (Wiley, 2000).

I estimated 24-hour rainfall thresholds for debris flows in study sites and dates that the 20 cm antecedent rainfall requirement was exceeded (Table A20). While the antecedent rainfall requirement was exceeded in early to mid-November in all sites, the 24-hour precipitation thresholds were not exceeded (Tables 2 and A20). Two landslides did occur in WRT in response to a storm that precipitated 49 mm on 4 January 2022, which is well below the calculated threshold (Table A20). The landslides occurred in a burned area and were initiated from road fill failure, suggesting that the combined effects of wildfire and road development lowered precipitation thresholds for landslides. In summary, this analysis indicates that published precipitation thresholds for debris flows were not exceeded during the study period, reiterating the caveat that Wiley's (2000) suggested thresholds do not consider wildfire. This analysis also highlights the critical need for development of post-fire debris flow thresholds in western Oregon, particularly given projected increases in fire frequency and severity across the Pacific Northwest under climate change (e.g., Halofsky et al., 2020; Littell et al., 2018).

Table A20. Precipitation thresholds for landslides/debris flows in study sites, calculated using PRISM (2022) data.

	Date of 20 cm Antecedent Rain		24-hour Precipitation
Site	WY 2021	WY 2022	Threshold[a] (mm)
WRT	11/16/2020	11/7/2021	123
BOG	11/16/2020	11/10/2021	113
SWP	11/15/2020	11/5/2021	137
CON	11/11/2020	11/5/2021	147
MCR	11/11/2020	11/5/2021	145

[a] Calculated as 40% of mean December rainfall (Wiley, 2000).